Conflict detection in a sequential decision task is associated with increased cortico-subthalamic coherence and prolonged subthalamic oscillatory response in the beta band

Author List:

Zita Eva Patai[1,2], Tom Foltynie[3], Patricia Limousin[3], Harith Akram[3], Ludvic Zrinzo[3], Rafal Bogacz[2]*, Vladimir Litvak[1]*

[1]Wellcome Centre for Human Neuroimaging, UCL Queen Square Institute of Neurology, London, UK, [2]MRC Brain Network Dynamics Unit, Oxford University, Oxford UK, [3]Functional Neurosurgery Unit, The National Hospital for Neurology and Neurosurgery and Department of Clinical and Movement Neurosciences, UCL Queen Square Institute of Neurology, London, UK

*Equal contribution

Abstract

Making accurate decisions often involves the integration of current and past evidence. Here we examine the neural correlates of conflict and evidence integration during sequential decision making. Patients implanted with deep-brain stimulation (DBS) electrodes and age-matched healthy controls performed an expanded judgement task, in which they were free to choose how many cues to sample. Behaviourally, we found that while patients sampled numerically more cues, they were less able to integrate evidence and showed suboptimal performance. Using recordings of Magnetoencephalography (MEG) and local field potentials (in patients) in subthalamic nucleus (STN), we found that beta oscillations signalled conflict between cues within a sequence. Following cues that differed from previous cues, beta power in the STN and cortex first decreased and then increased. Importantly, the conflict signal in the STN outlasted the cortical one, carrying over to the next cue in the sequence. Furthermore, premotor cortico-subthalamic beta coherence increased during the initial power decrease. These results extend our understanding of cortico-subcortical dynamics of conflict processing, and do so in a context where evidence must be accumulated in discrete steps, much like in real life, leading to a more nuanced picture of conflict monitoring systems in the brain and potential changes due to disease.

Introduction

Whether it is deciding which method of transportation to take to get to work most efficiently or which horse to bet on to maximize monetary gain, humans are constantly integrating noisy evidence from their environment and past experience, in order to optimize their decisions and to choose the most appropriate action. Often the information comes at intervals, thus necessitating a system that can track incoming signals over time and only commit to making a choice after sufficient evidence has been integrated (1–3). The details of how and where the brain determines if the evidence is sufficient are largely unknown, but it is thought that this process relies on the cortico-basal-ganglia circuit (4). Research in human patients with implanted electrodes for clinical deep-brain stimulation (DBS) treatment has pointed to the role of the subthalamic nucleus (STN) of the basal ganglia as a decision gate-keeper. The STN is postulated to set the decision threshold in the face of conflicting information (5). This theory suggests that in situations of conflict between competing responses, the STN activity postpones action initiation until the conflict is resolved. As predicted by the model, STN activity is increased for high conflict trials and STN-DBS affected decision making when faced with conflicting evidence (6–8). Furthermore, the decision threshold correlated specifically with changes in STN theta oscillatory power (9,10). The overarching proposal is that oscillatory activity, primarily in the theta and beta bands, in the basal ganglia, reflects immediate inhibition to motor output during situations involving conflict (5), whether it is response, sensory or cognitive uncertainty (11).

The majority of previous studies in the STN employed paradigms in which the putative processes of conflict detection and setting of decision threshold happened in close temporal proximity. For example, in previously used paradigms such as the flanker task (Zavala et al., 2015), go-no-go (Alegre et al., 2013; Benis et al., 2014), and Stroop task (Brittain et al., 2012) evidence was presented simultaneously. Although STN activity was also studied in random dot motion paradigm that required evidence accumulation over time (18), it was unknown exactly what sensory evidence was presented on individual trials due to the noisy nature of stimuli and, importantly, conflict was time-limited. As a result, previous studies do not allow us to fully disentangle the temporal sequence of the different neural correlates of ongoing evidence accumulation and conflict during decision making. In particular, it is not clear to what kind of

conflicting information during evidence accumulation the STN responds: does it respond to a local conflict, when a new piece of information does not match single previous piece in the sequence, or does it respond to a global conflict, when a new piece of information does not match overall evidence from the entire trial? This is particularly relevant as patients with Parkinson's disease on medication and with DBS often show pathologically increased impulsivity in the face of conflict (19–21), and new evidence suggests that these changes could be due to the stimulation affecting specific cortico-subthalamic networks (22).

An important role in shaping the STN activity is played by the interaction between the cortical circuits and the STN. However, the nature and cortical locus of this interaction has only been examined in a handful of studies. Resting-state coherence between the STN and ipsilateral frontal cortex has shown a peak in the beta band in human patients (Litvak, Jha, et al., 2011; West et al., 2020) as well as rodent models of Parkinson's disease (24,26). Additionally, coherence in the theta band from frontal sites (as measured with electroencephalography) to the STN increased during a conflict detection task (27,28).

To precisely characterize how the neural activity in cortex and the STN changes during the process of evidence accumulation, we recorded STN local field potential (STN-LFP) simultaneously with whole-head magnetoencephalography (MEG) while Parkinson's disease patients performed an expanded judgement task (29). Here, cues are presented at discrete intervals within a trial sequence and evidence for the correct answer develops as the participant samples and integrates multiple cues (Figure 1). This paradigm allowed us to investigate how behavioural and neural responses depend on the continual unfolding of evidence extended in time, determine what kind of conflicting information the STN responds to, and test predictions of computational models.

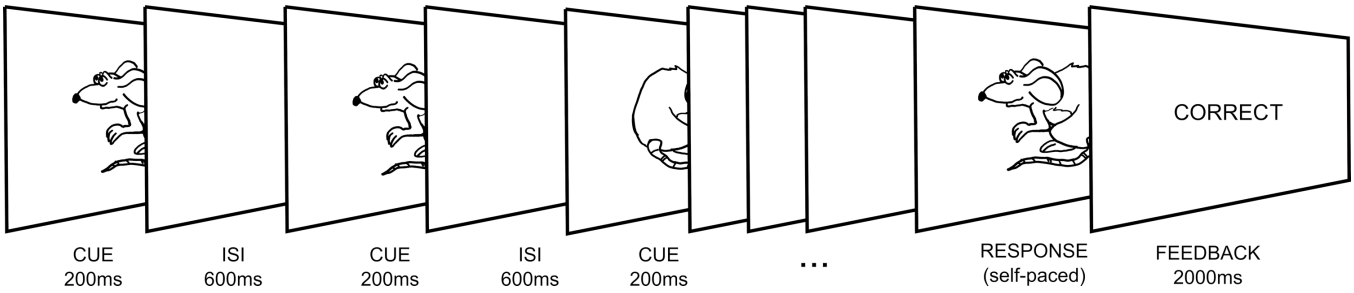

Figure 1: Expanded Judgement Task. Participants performed a version of an evidence integration task, with two key elements: 1. the cues were presented sequentially within the trial rather than simultaneously, which allowed us to examine evidence accumulation over time, and 2. The trial duration, i.e. number of cues sampled, was up to the participants, who responded when they felt they had received enough information to make a decision. Participants were required to guess the likely direction (left or right) the mouse 'would run' in. Each cue was 70% valid, i.e. they represented the correct direction 70% of the time if they were to be treated in isolation.

Results

Patients are able to accumulate evidence over time

Patients waited on average 6.6 stimuli before making a response (6.59±0.52 sem) and their accuracy was significantly above the 70% level expected if they only based their decision on a single cue (80±0.03 sem, t=3.6, p=0.004). Controls waited on average 6.3 stimuli before making a response (6.29±0.46 sem) and were above 70% in their accuracy (88.6±0.01 sem, t=18.4, p<0.001). There was no significant difference between groups in the number of stimuli viewed before making a choice (t=0.42, p-value = 0.68), but patients had lower accuracy (t=-2.99, p=0.0009) and slower reaction time (as measured from the onset of the last cue before a response was made, t=2.16, p=0.041). To explore potential strategies participants could have used in the task, we compared performance in both groups to an agent that would have been an optimal observer, and would choose to respond left if the number of left cues was higher than the number of right cues, to respond right for a larger number of right cues, and would choose randomly if the numbers were equal. In other words, for each participant, we calculated the accuracy they would have achieved had they integrated evidence optimally, but we used the stimuli sampled by the participant on each trial. We found that controls and patients had significantly lower accuracy (controls: p=0.019, patients: p=0.0076) than an ideal observer would have, based on the same cue sampling (89%

for controls and 87% for patients). Next, we asked whether participants were just solving the task by responding after they spotted two of the same stimuli in a row (i.e. after the first 'same' pair). We permuted all the possible stimulus sequences that were used in the experiment 100,000 times, calculated the accuracy of an agent that would commit to a choice after the first pair is seen (e.g. left-left), and found the limit to be 80.6%. While patients were not significantly different ($p>0.1$), controls did perform better than this strategy would suggest ($p<0.001$). Nevertheless, analyzing behavioural data with explicit mathematical models demonstrated that the patients were not using the strategy of responding after two same cues only, but rather relied on imperfect evidence accumulation. See Supplemental Material for details.

STN beta power shows persistent activity to local conflict during evidence accumulation

In order to investigate how the STN represents the inconsistencies when faced with conflicting evidence, we separated all cues into two categories: 'same' or 'different' to the one immediately before it (we term this 'cue i', Figure 2A). In our analyses of neural responses to cues, we excluded the first cues in a sequence, because it is not possible to classify them as 'same' or 'different', and last cues seen as they overlapped with the response period. Thus, if a participant experienced this sequence of mouse images: 'left-right-left-left-right', the analysed conditions would be 'different-different-same'.

We found that only beta oscillations responded to local conflict, generating a significant difference between 'same' and 'different' cues (cue 'i' in Figure 2B left panel) starting around 100ms after cue onset. Beta also showed a significant difference in the subsequent cue (i+1), with 'different' cues showing an increase in beta power, thus conflicting information on cue i results in increased beta power on cue i+1 (see Supplementary Figure 2 for details), a pattern of activity that is consistent with response inhibition (significant time clusters: 100-450ms, 750-1100ms, 1300-1600ms). These effects were greatly reduced in the theta band, with an effect of condition only briefly detectable during cue 'i+1' (Figure 2B-C, right panel).

We did not find a relationship between behaviour on the task and these neural effects (see Supplemental Material Table 2).

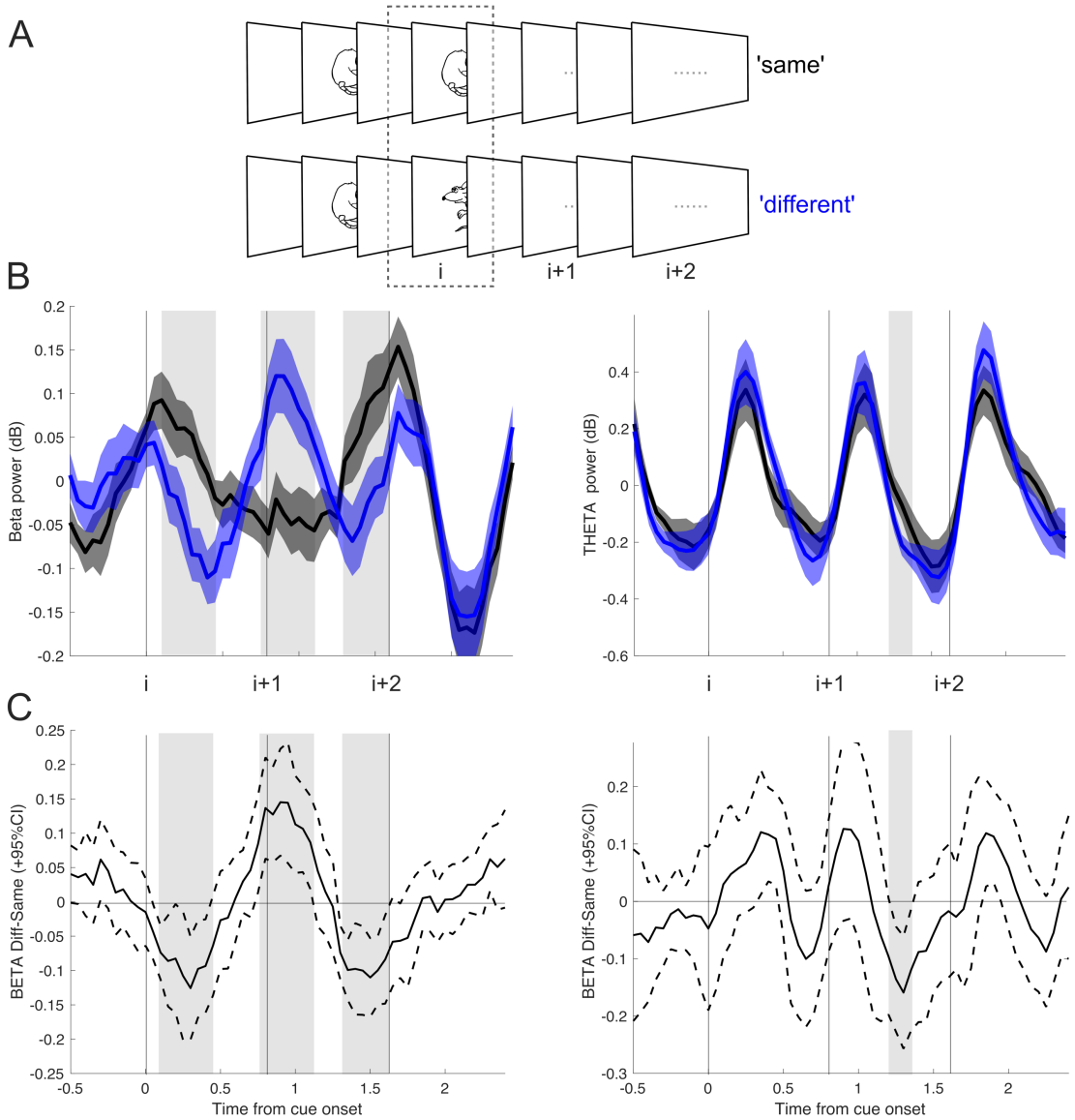

Figure 2: Beta signalled local conflict, and carried over this effect to the next cue in a sequence. A) Notation used in the paper. Let us consider an arbitrary cue i in a sequence, where i>1: If cue i-1 is the same as cue i, then we would call this the 'same' condition, and 'different' otherwise. We also plot the subsequent cues (i+1, i+2) for carry-over effects, but these are collapsed across cue type, left or right (see Supplemental Figure 2 for more detail). B) Left panel: Beta carried information locally as well as over to the next cue, with increased beta power for the 'different' condition. Right panel: Theta only carried mismatch information at the next cue in the sequence. Significant time periods are highlighted with shaded grey bars. Vertical lines show onset of cues in the sequence. The shaded error bars show standard error of the mean. C) Difference waves of conditions ('different' minus 'same') with 95% confidence intervals shown by the dotted lines. After an initial dip there is a clear increase in beta power following the conflicting cue (i) starting just before the onset of cue i+1. Significant time periods are highlighted with shaded grey bars copied from panel B for comparison. Note that the apparent onset of the effect before zero is due to limited time resolution of the time-frequency decomposition.

Cortical activity reflects rapid but non-persistent local conflict detection

We investigated sensor-level MEG signals from controls and patients in response to local conflict detection within the sequence. As with the STN, widespread activity over central sensors was found to signal local conflict – with an initial dip followed by an increase in beta power on 'different' trials (Figure 3). This effect was significant in controls (50-400ms, 11-28 Hz) and when combining the two groups (0-350ms, 11-22Hz) but not in patients alone. This may be due to the non-optimal positioning in the MEG helmet for the patient group, which was dictated by the need to accommodate externalized DBS leads and connectors. Despite the effect of conflict not being significant in patients, its time course at the source level was similar in both groups (see below). Importantly, the time-course of the cortical effect was quicker than that of the STN (Figure 2B), with conflicting information not persisting until the onset of the next cue in the sequence.

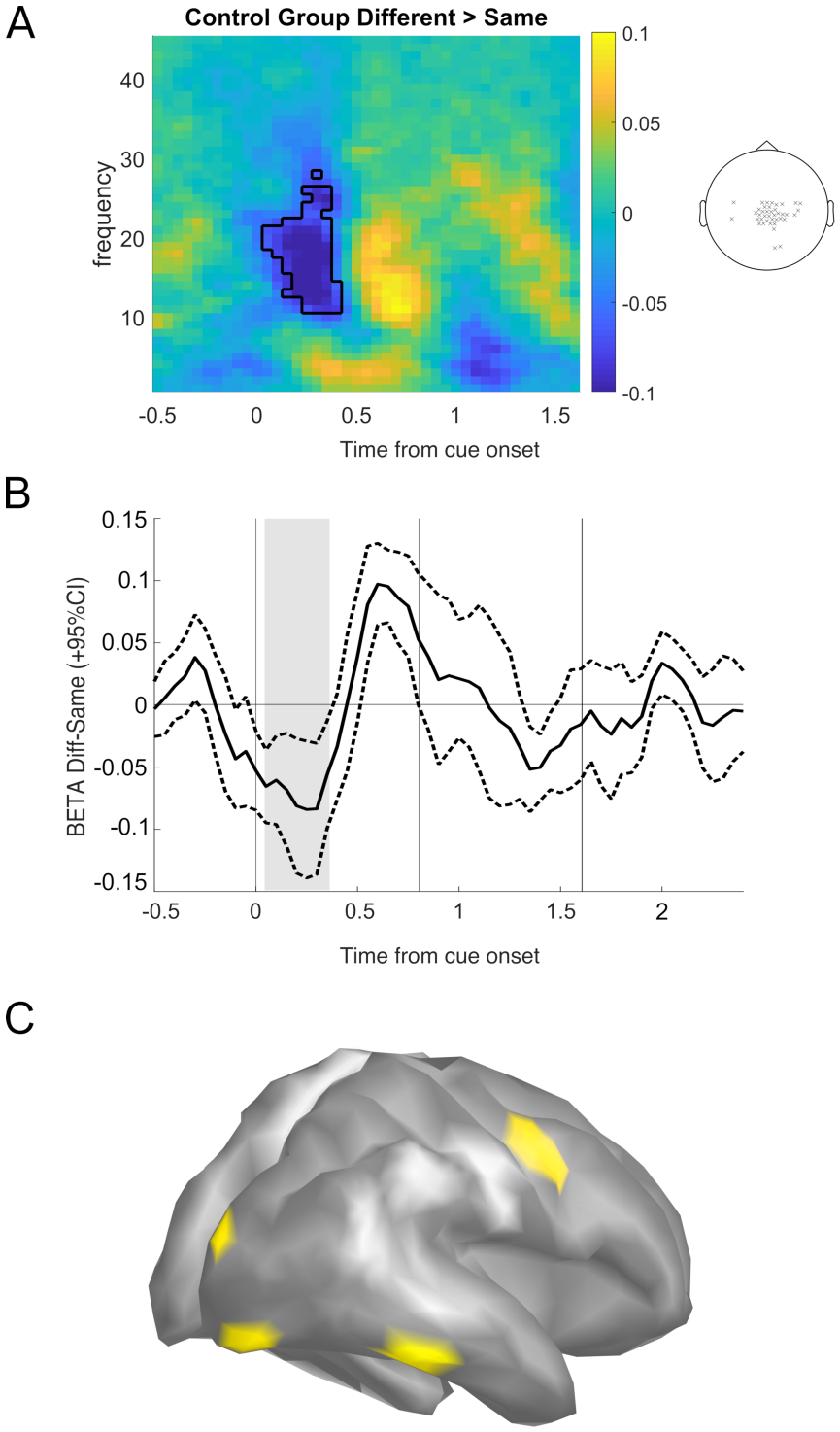

Figure 3: Cortical activity to local conflict parallels STN but peaks earlier on average and has a shorter time course. A) Top: Time-frequency plot showing significant times and frequencies when contrasting 'different' vs 'same' cues. Significant channels are shown on the right. B) Difference wave for the beta (13-30Hz) band, as represented in Figure 2B. The dotted lines indicate 95% confidence intervals and the significant time period (the same as in A) is highlighted with shaded grey bars. Note that the apparent onset of the effect before zero is due to limited time resolution of the time-frequency decomposition. C) Source localization placed these effects in three right-lateralized areas: occipital pole, ventral temporal cortex and premotor area BA6.

Coherence is increased between STN and frontal cortex during local conflict

We used beamforming in a combined sample of patients and controls to localize the source of the 'same-different' effect (averaged over: 200-400ms, 10-31Hz), and found four right-hemisphere lateralized peaks (Figure 3C): occipital pole (2 peaks: MNI 59, -53, -21; 35, -89, -16), ventral temporal cortex (MNI 19, -98, 14) and premotor cortex/BA6 (MNI 52, -7, 44). Next, we measured in patients the coherence between these cortical vertices and both the left and right STN-LFPs, separately. The coherence spectra were averaged over adjacent vertices resulting in 3 cortical sources. We found a significant increase in coherence between the right frontal cortex and the right STN (Figure 4) in the beta band (17-21Hz), shortly after the onset of 'different' cues (0-240ms), suggesting that ipsilateral cortical-subthalamic coherence is increased in the face of local conflict in the right hemisphere. No other sources, nor the left STN showed any significant effects.

To further investigate how localization of electrodes within the STN and surrounding areas may influence our findings, we reconstructed the electrode locations (see Figure S3a and Supplementary Methods) and found that the strongest coherence effect was seen for the middle electrode pair (Right 1-2, see Figure S4), which is in line with studies showing that beta power is strongest in the motor subdivision of the STN (30), and in the areas more superior to the surgical target (31). A recent study (32) also showed that beta activity was detected in monopolar recordings when any portion of a macrocontact was within the microelectrode-defined STN border. We would, therefore, expect that for bipolar recordings as in the present study, the strongest signal i.e. voltage difference, would be obtained for pairs with the midpoint close to STN border. We indeed found that the midpoint of contact pair Right 1-2 was within 0.5 mm (one contact length) from the nearest STN voxel for all patients and within 0.5 mm from the nearest voxel in the motor subdivision of the STN in 12 out of 13 patients. These results are based on DISTAL DBS functional zones atlas (33)) and should be interpreted with caution as normalisation of subcortical anatomy to the template space does not always perfectly capture the variability of individual STN shapes.

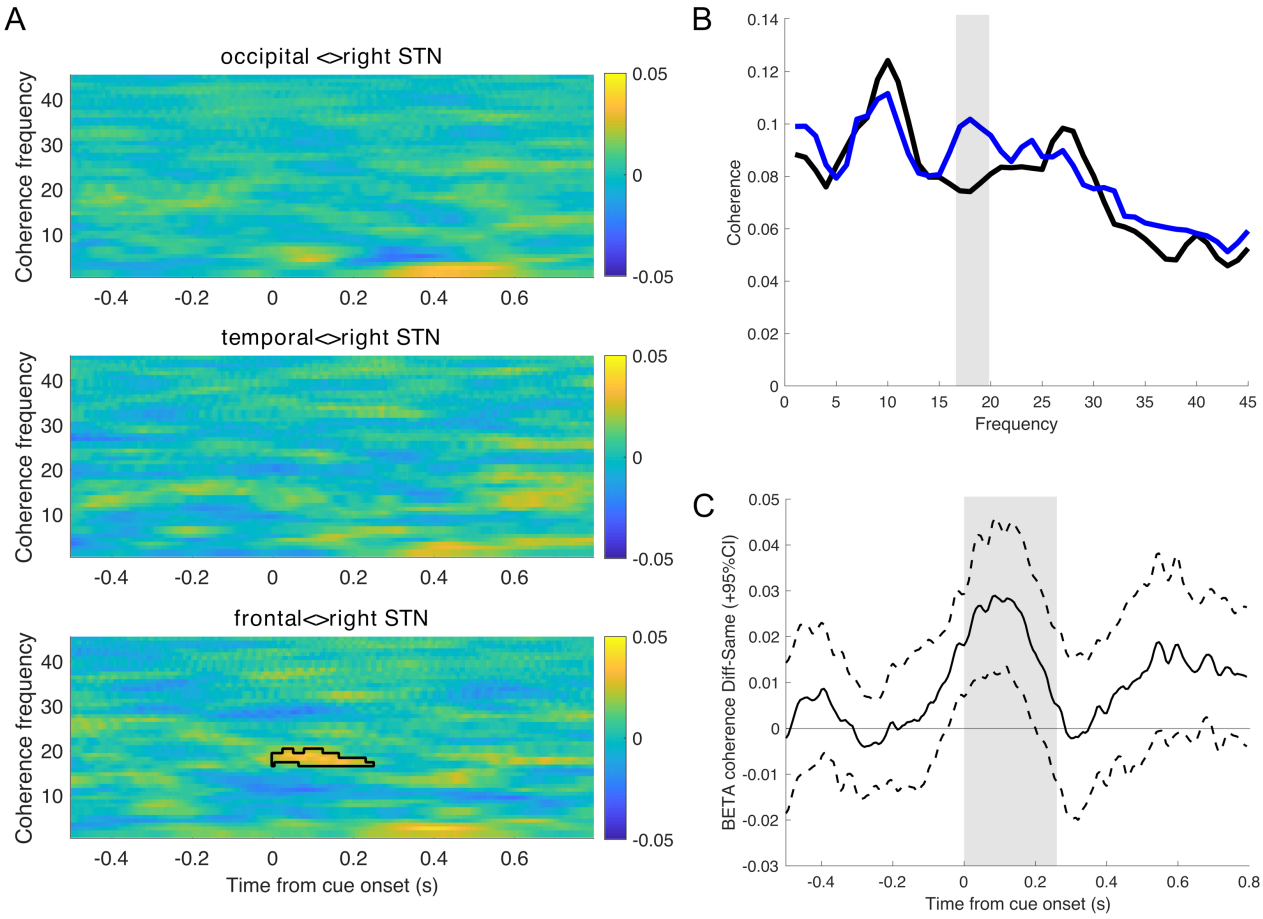

Figure 4: Increased coherence between right frontal cortex and right STN during local conflict. A) Plotted are the time-frequency plots of coherence between the right STN and the three cortical sources (all right-lateralized). Beta coherence is increased for the 'different' condition, for 0-240ms after cue onset. B) Frequency spectra of 'same' (black) and 'different' (blue) trials during the significant time period from A. Grey area highlights significant frequencies: 17-20Hz. C) Time-course of coherence plotted as a difference wave between conditions. The dotted lines indicate 95% confidence intervals and the significant time period is highlighted with shaded grey bars (0-240ms). Note that the apparent onset of the effect before zero is due to limited time resolution of the time-frequency decomposition.

Other variables related to decision making

In addition to local conflict, we analyzed whether other variables occurring in theoretical models of decision making were reflected in neural activity. First, we explored if STN represents the normalization term in Bayes theorem as proposed in a previously suggested computational model (34). This model predicts that the activity in STN is proportional to a logarithm of the normalization term in Bayes theorem ln P(cue i). This probability is computed on the basis of all previous cues {cue 1 , …, cue i-1} so it expresses how expected the current cue is given all cues seen before. The negative of this regressor, -ln P(cue i), is equal to Shannon's

surprise, so it expresses how much cue i disagrees with overall information in all previous cues, and hence it could be viewed as a measure of global conflict. Therefore, by investigating the correlation between the normalization term ln P(cue i) and LFP activity we can test two separate hypotheses: a computational model (34) predicts a positive correlation, while a hypothesis that STN responds to global conflict predicts a negative correlation. We tested if the normalization term affects power of beta oscillations in the STN and did not find evidence supporting any of these two hypotheses in our data (Figure 5A; details of methods in Supplemental Methods).

It has been previously reported that the Bayesian normalization term was encoded in the power of beta oscillations in the cortex in a decision task in which the evidence was also presented gradually (35). Consequently, we explored whether there was any coding of the Bayesian normalization term in the cortex, by running a regression across all times, frequencies and channels, with cue identity (‘same’ or ‘different’) as a control variable. We found a significant effect in the beta band towards the end of the cue period (Figure 5B), matching in timing and frequency to those reported by Gould et al. (2012).

We also explored whether there was a signal reflecting the magnitude of accumulated evidence in the STN and cortex, but we did not find such a signal (STN: Figure 5A, cortex: not shown). Finally, given previous reports of decreasing beta power as a result of increasing working memory load (36), we also ran a regression on beta power including the serial position at each cue stimulus, and found no significant effects (see Figure 5A, ‘stimulus number’). Instead as can be seen in Figure 5A, beta power carried information about the similarity of the stimulus to the previous one (‘same’ or ‘different’), but no signal pertaining to of any form of evidence accumulation. There were no significant effects of any of the above regressors on theta power.

A traditional view of the STN places a role on theta power in the process of setting decision thresholds in the face of conflict - in our paradigm we could directly test whether this threshold had a behavioural correlate, namely the number of samples seen before committing to a response. We divided the second cue in a sequence into two conditions again: ‘same’ or ‘different’ as the first cue in the sequence. Behaviourally we found that indeed participants sample more evidence (or make more

‘draws’) after an initial ‘different’ stimulus pair (mean samples after different: 5.07, mean after ‘same’: 4.8, p=0.007). We ran a regression between theta power at the second stimulus (i.e. first possible point of conflict) and the number of stimulus ‘draws’ thereafter, in other words the number of stimuli viewed before a response was made. If indeed theta sets a threshold for subsequent decision making, then we would predict that theta should scale with the number of upcoming stimuli, which can in turn be viewed as a proxy for the amount of evidence needed to make a decision. We found that theta power after the second cue was related with the number of stimuli subsequently seen before choice, such that lower theta after a ‘same’ cue resulted in more samples drawn, and this was lower than theta power after ‘different’ cues (between 300-400ms after cue onset). However, this effect did not survive cluster correction for multiple comparisons across the cue period (p>0.1). No such relationship was found for beta power.

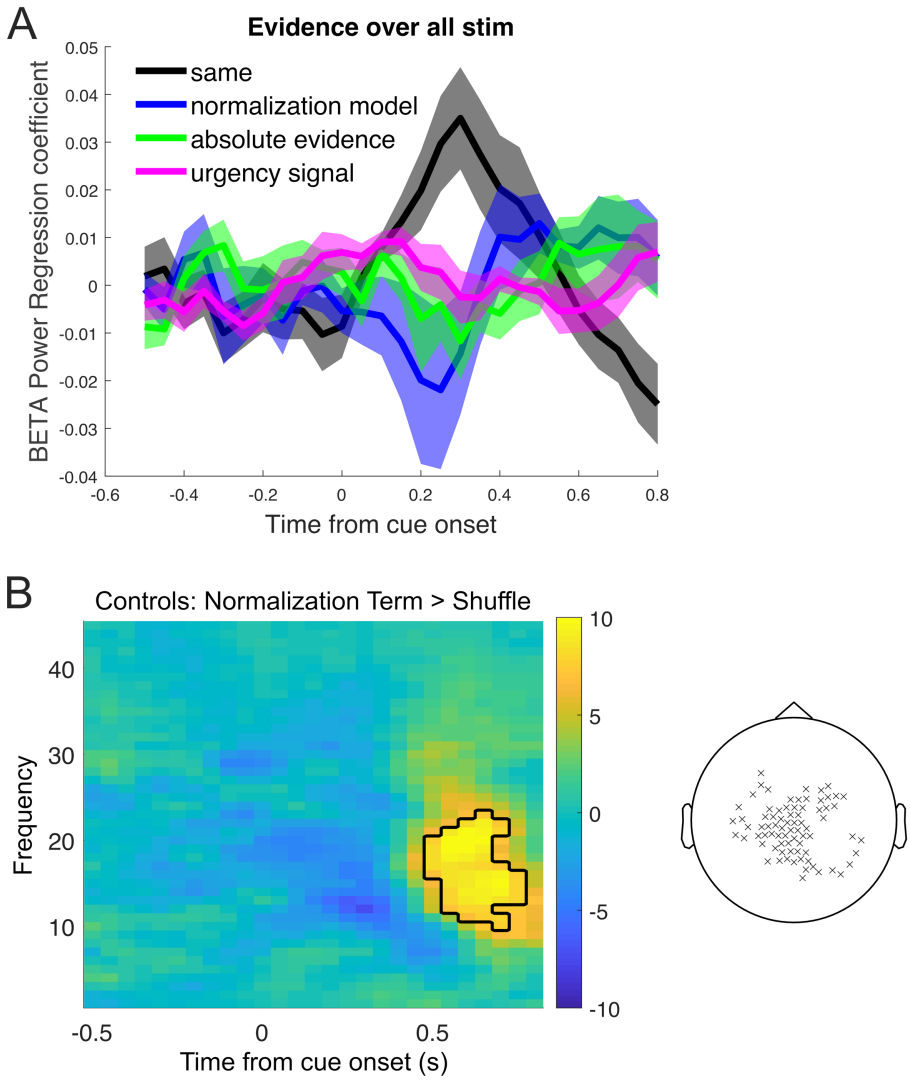

Figure 5: STN activity encodes local conflict via beta oscillations, but does not code variables related to accumulation of evidence. A) A linear regression of beta and theta in the STN revealed that the only clear signal was related to the identity of the cue ('same' or 'different', shaded in grey) in beta power only, and there was no encoding of Bayesian normalization, as proposed previously (34,37), nor was there encoding of integrated evidence, or stimulus number in the sequence of cues in a trial. **B)** We found evidence for the Bayesian normalization term in controls at the sensor level reproducing the result of Gould et al. (2012).

Discussion

In this experiment we present novel evidence pertaining to the role of the STN and cortico-subthalamic communication during sequential decision making, using a task in which participants had to integrate evidence over discrete time periods, with no constraints on how many samples they could observe before making a decision. We find evidence for persistent local conflict representation in the STN via beta oscillations, and increased coherence with frontal cortex.

Representation of Conflict in the STN

We found that activity in the beta band carried information about local conflict, i.e. a difference between the current cue and the preceding one, but not about global conflict i.e. a surprise by the current cue given all previous cues. Although we established that beta power varies depending on whether the current cue differs from a previous one in a sequence – an event to which we refer as a local conflict – it is less clear from our data what the function of this activity is, and what fundamental variable it encodes.

It is possible that the observed changes in beta power are connected with motor inhibition. Beta power was initially lower for cues that were 'different' to the one immediately before and continued to increase across the next cue in the sequence. Hence one can interpret the increase of beta power as a stop signal, or a break on motor output (14) inhibiting a response after an inconsistent cue. Moreover, the majority of trials ended on a 'same' cue (Supplementary Table 1), which is in line with an overall increase in beta synchronization after 'different' cues and lower probability of responding.

The response to different cues could also be interpreted as encoding of expectancy valuation, uncertainty or surprise. Beta power increases have been reported when a 'surprise' stimulus is presented (38), and STN activity measured with fMRI has been shown to increase when there is increased uncertainty which option is correct arising due to too much choice (39) – though this has been shown on singular events rather than over the course of evidence accumulation. Validating such interpretations is difficult when they are expressed just in words, and hence it is important to define them mathematically, so such quantities can be computed at individual moments of time and compared with the data. For example, in our study we have investigated if Shannon's surprise is encoded in STN activity, but found no evidence for it.

It is also worth relating observed STN activity with results of previous studies. It has been shown before that activity in the beta band carries conflict information across trials (40), but we also show this effect within a trial, as conflict arises within the sequence of evidence. As for the initial decrease in beta power, this has been reported before as a slower 'resynchronization' of beta during incongruent cues (16), and also as a pathological signal inhibiting the integration of melodic sequences (41).

Interaction between STN and Cortex

Interestingly, the overall picture was very similar in cortex, with two main differences: the 'same'-'different' effect on average peaked earlier in the cortex (Figure 6), and also did not carry over to the next cue in the sequence (Figure 3A). A possible interpretation is that the cortex signalled the immediate local conflict to STN, dovetailing with recent evidence suggesting the cortical conflict signal precedes the STN (42), which then maintained a more persistent activity to inhibit responses (16,43). Brief cortical beta responses triggering a prolonged STN response are in agreement with the suggestion that the cortex initiates abnormal subcortical beta activity that is then amplified by the subthalamo-pallidal circuit (44), or that beta power represents post-decision stabilization of cortico-basal ganglia circuits (45).

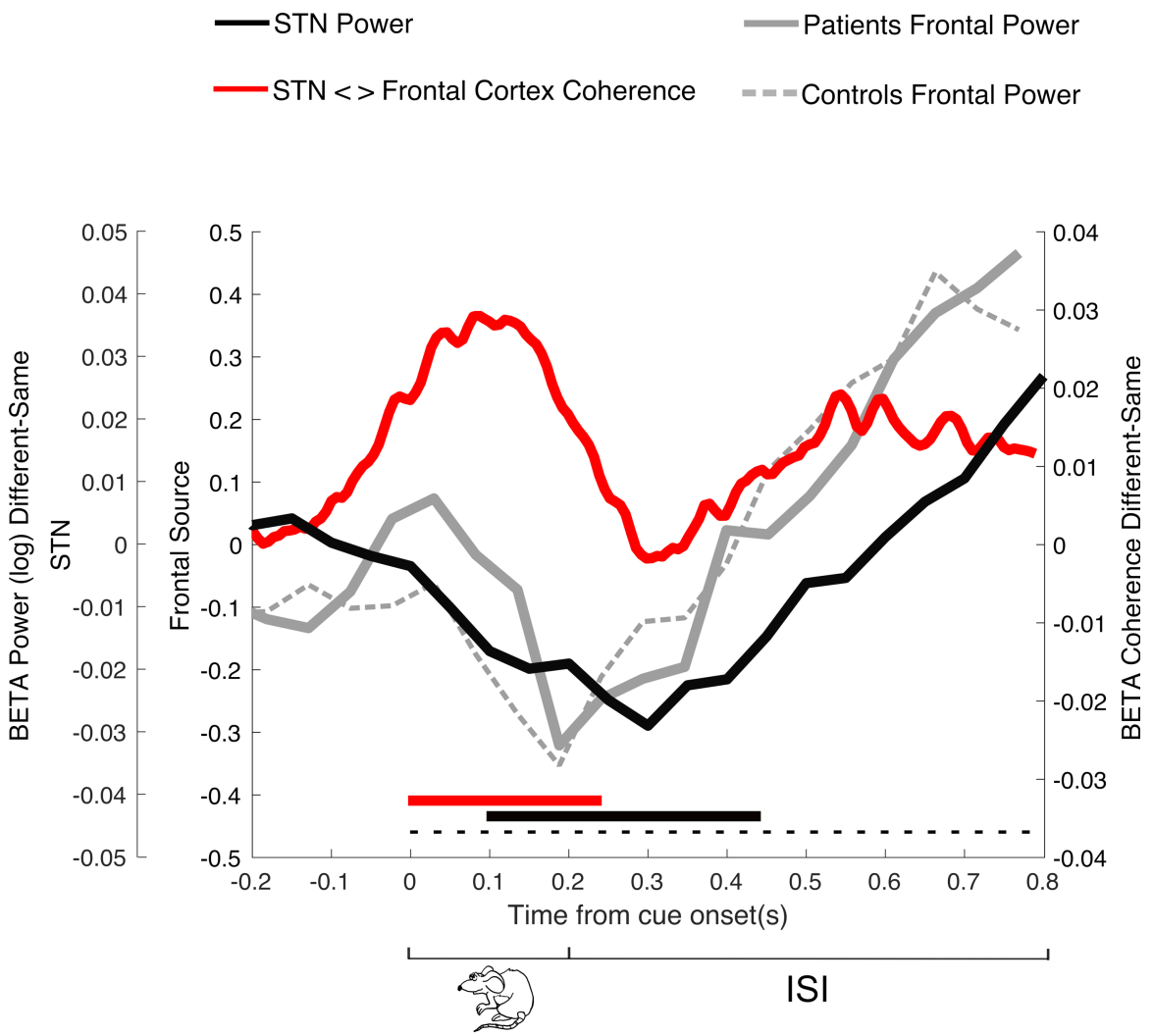

Figure 6: Time-course of beta power and coherence differences between conditions. This figure shows a summary of findings presented in Figure 2C and 4C as well as source power time courses to facilitate the comparison of timings of the effects. While the STN LFPs, sensor-level MEG signal (not shown) and the beamformed frontal source in patients and controls all show a decrease in beta power immediately after 'different' cues (onset at zero seconds), the beta coherence between the STN and frontal cortex (red line) shows a concurrent increase. Of note is that the cue was on screen for 200ms (out of total SOA of 800ms, ISI 600ms), which is the time window similar to that in which significant coherence increase was found. Coloured lines at the bottom of the plot indicate the times of significant differences between 'same' and 'different' cues for each measure plotted, red: right STN- right frontal coherence, black: STN power, dotted: MEG sensor level power (time course not shown). The frontal source was not submitted to separate statistical testing as it is derived from the MEG sensor data. Note that the apparent onset of effects before zero is due to limited time resolution of the time-frequency decomposition.

When we localized the sources of the ‘same’-‘different’ effect, we found three right-lateralized areas in the cortex which showed a local conflict signal: occipital, temporal and frontal cortex. Only the frontal source, located in premotor cortex/supplementary motor area (BA6) showed a significant coherence modulation with the ipsilateral STN only, namely an increase in beta coherence at the onset of a ‘different’, or conflict, cue (Figure 4). Critically, this is in contrast to the overall *decrease* in beta power during most of this time period, both in the STN and the cortex (Figure 6) ruling out ‘power confound’ as a possible explanation (46). It may seem surprising that the increase in coherence in patients coincides (at least partially) with a decrease in power. This is perfectly possible, however, because coherence increase can be driven purely by changes in phase synchronisation that do not require an increase in power and can even coincide with a power decrease as long as oscillatory activity is not completely supressed.

Due to the cortico-STN coherence having a short time course, we were unable to reliably estimate the directionality of coherence, but previous reports on resting-state data have shown cortex to drive STN activity (23), which is in line with the finding here that the ‘same’-‘different’ effect seems to peak earlier in the cortical signal. However, recent data has also suggested that during processing of incongruent stimuli, STN to primary motor effective connectivity is increased in the beta band (47), suggesting that the directionality of communication may be different across task and non-task contexts.

The right BA6 is well-established as a cortical region involved in response-inhibition/initiation and cognitive control (48–50). A recent study (22) has shown that increased impulsivity post-DBS is associated with the stimulation affecting specific cortico-subthalamic networks. These include supplementary motor area (SMA)/BA6 (albeit in the left hemisphere) and right ventro-medial prefrontal cortex (vmPFC). We have previously shown (Oswal et al. 2016) that DBS decreases cortico-subthalamic coherence, likely by disrupting the activity of cortical areas, directly connected to the STN, via antidromic spike propagation. Taken together, these results could suggest that DBS disrupts non-pathological cortico-subthalamic communication (as manifested by increased coherence during conflict in the present study) and thereby leads to increased impulsivity.

While it is well-established that the cortex communicates with the STN via two anatomically defined pathways, the indirect and the hyperdirect pathways (51–53), recent evidence suggests the existence of two separate coherent beta oscillatory networks between the cortex and the STN (54) with the low beta network (13-21Hz) likely corresponding to the indirect pathway from lateral prefrontal regions to the STN via the striatum and external Globus Pallidus. Here we find evidence for a similar pattern of oscillatory connectivity, which may have implications for understanding the involvement of various pathways in sequential evidence accumulation. Interestingly, a recent study showed evidence of a hyperdirect pathway from inferior frontal gyrus (IFG) to the STN operating in the 13-30Hz range (42), which points to a more ventral portion of the frontal cortex than presented here. In fact, many studies in stop-signal/go-nogo tasks point to the IFG (55), however in these tasks conflict is not part of an evidence accumulation process, hence we may expect that different cortical regions interact with the basal ganglia, and STN, depending on the type of decision being made, as part of a distributed network (22,56,57). Although here our information about STN activity and cortico-subthalamic coherence comes from Parkinson's patients, one hypothesis that could be considered is that our experiment revealed an aspect of the healthy functioning of this circuit that is then hijacked by the disease resulting in the generation of abnormal STN activity that impairs movement.

Where is the theta conflict signal?

The predominant theory of STN function, and also that of the cortex during conflict detection, is the involvement of theta oscillations (58). A large portion of empirical findings on the STN shows that it carries conflict information via the theta band (9,10,12,27,36,40,59). Yet in our task we only found a weak effect of theta modulation, in the cue following a local conflict (cue i+1). This effect was present only in the STN, and no theta effects were found in the cortex. Moreover, this manifested as reduced theta synchronization to 'different' cues, which is the opposite of the standard reported theta increase during conflict. One explanation may be the task design, as it differs from previous paradigms: there are no long intervals over which to examine slow oscillations, such as theta. Our results, therefore, though focussed on theta power (2-8Hz), may be dominated by evoked potentials, as cues were presented in a fixed,

510 relatively short duration (200ms, with 600ms inter stimulus interval) sequence.
511 Additionally, here conflict is defined over the course of multiple cues, not on a singular
512 trial in isolation. Thus, the integration of conflict over time may in fact be driven by
513 different signals – beta may represent a more consistent inhibition during conflicting
514 incoming information. Nevertheless, others have also reported a lack of theta effects
515 in the STN during a stop-signal task (59).

516 In terms of STN connectivity, two previous reports have found increased theta
517 coherence during conflict with medial frontal cortex (27,28). We found increased
518 coherence in the beta band, and a more lateral frontal area. The other reports,
519 however, used EEG rather than MEG. This might be critical in our case as MEG is
520 known to be less sensitive to the anterior cingulate theta conflict signal that most of
521 the authors consider to be the source driving theta responses in the STN. This could
522 be due to higher variability of the MEG theta conflict signature topographies that do
523 not survive averaging across subjects and require a different kind of analysis
524 approaches (60). Additionally, neither of these reports investigated changes in beta
525 coherence, and thus it is unclear whether these effects existed at all. Finally, the
526 previous reports analysed coherence during a cue period that was uninterrupted by
527 additional incoming stimuli (as is the case in our task), and thus low frequency
528 oscillations may be clearer in those studies, as discussed above.

529 *Updating models of the STN*

530 The role of the STN in decision making has been formalized in several computational
531 models that account for a range of findings related to anatomy and physiology of the
532 cortico-basal ganglia circuit including the STN. An influential model proposed by Frank
533 (2006) suggests that in situations of conflict between competing responses an
534 increased activity of STN postpones action initiation (5). This model proposes that STN
535 is essential for decision making since it ensures that an action is only selected when
536 it has high evidence, relative to the other options. Another model proposed by Bogacz
537 & Gurney (2007) suggests that the basal ganglia compute the reward probabilities for
538 selecting different actions according to Bayesian decision theory (34,61). According to
539 that model, STN computes the normalization term in Bayes theorem, which ensures
540 that the updated probabilities add up to 1 across the actions. While in our task we did
541 not find conclusive evidence that the STN is encoding Bayesian normalization (Figure

542 5A), we observed its participation in conflict processing, yet not in the predicted theta
543 frequency band (see previous section). It is important to remember that, despite being
544 on medication, these experiments were performed in patients whose neural circuitry
545 has been affected by advanced Parkinson's disease. Control participants did show
546 activity encoding Bayesian normalization at the cortical level (Figure 5B), in agreement
547 with a previous study (35). In fact, the timing and frequency of this activity was
548 remarkably similar to that found by Gould et al. in a more complex paradigm (cf. their
549 Figure 8). Thus, one cannot rule out the possibility that the Bayesian normalization is
550 encoded by the STN of healthy individuals, but testing this hypothesis would require a
551 different experimental technique (e.g. recording of STN neural activity from animals
552 during an analogous decision making task, such as a task employed by Brunton,
553 Botvinick, & Brody, 2013). An alternative explanation is that the Bayesian
554 normalization term is computed not in the STN but elsewhere. However, this
555 computation requires a highly specialized circuit and it is unclear where else such
556 circuit could be located in the brain. Recent evidence suggests that subdivisions within
557 the STN may be responsible for different types of inhibition, with prepotent response
558 inhibition to cues (go-no-go task) being more dependent on the ventral portion of the
559 STN, while general motor symptoms of Parkinson's are dependent on a wide area of
560 the STN (63). Given that the majority of our recording sites were well within the dorsal
561 ('motor') region of the STN, we cannot rule out the contribution of more ventral sites
562 to these computations.

563 We did not find encoding of pure evidence integration or response certainty, as in
564 previous reports (35,64,65). Furthermore, our behavioural modelling revealed that
565 both patients and controls were using an imperfect form of evidence integration to
566 make their responses, with patients specifically sampling more cues and still
567 performing worse than controls. Given that we were unable to measure ongoing eye-
568 movements during task performance – which would have provided a clearer picture of
569 attention to the individual cues – it is hard to tease apart which individual cues *actually*
570 contributed to the decision. Nevertheless, whether patients sampled more cues
571 because of decreased attention to each cue, a difficulty in keeping track of cues due
572 to reduced working-memory, or due to increased impulsivity, these results highlight
573 imperfect evidence integration in patients.

574

575 **Conclusion**

576 Contrary to the emphasis on theta signals in the context of immediate conflict, here
577 we find a prominent role for beta oscillations in signalling local conflict in a sequence
578 of evidence. We find that both cortex and the STN carry this signal, with cortex peaking
579 on average earlier, and find that coherence is increased between these areas when
580 local conflict is detected. We showed that a brief cortical response to local conflict in
581 the cortex triggers a more prolonged response in the STN, which could be an aspect
582 of the healthy function opening the door to pathological amplification of STN beta in
583 Parkinson's.

584 **Methods**

585 *Participants*

586 We tested 15 patients with a clinical diagnosis of Parkinson's disease (14 male, mean
587 age: 59, range 47-71, two left-handers), following electrode implantation for DBS
588 treatment, before full closure of the scalp, thus allowing for intracranial recordings of
589 the STN (all bilateral recordings, except 1 patient right unilateral and 1 patient with 3
590 contacts in the left STN and only 2 on the right, this patient was also subsequently
591 diagnosed with Multiple Systems Atrophy). Among tested patients, 11 had Medtronic
592 3389 electrodes, while 4 had Boston Vercise™ directional leads. The surgical
593 procedures are described in detail in (66). All patients were assessed on medication
594 (mean Levodopa Equivalent Dosage 1272mg, range: 500-1727.5mg). Unified
595 Parkinson's Disease Rating Scale (UPDRS) part 3 scores were 39.6±14
596 (mean±standard deviation, range: 18-61) when OFF medication, and 15.4±6.5 (range:
597 7-30) when ON medication. None of the patients had cognitive impairment (Mini–
598 Mental State Examination (MMSE) scores: mean 28.8, range: 26-30, one patient score
599 missing), clinical depression, or apathy. Two patients were excluded from the analysis
600 due to poor performance of the task (see *Task* below). We recruited 13 age and gender
601 matched controls (12 male, mean age: 57, range 44-70, two left-handers). The patient
602 study was approved by the UK National Research Ethics Service Committee for South
603 Central Oxford and the control study was covered by University College London Ethics
604 Committee approval for minimum risk magnetoencephalography studies of healthy
605 human cognition. The patients did not receive financial compensation and the controls
606 were compensated for their time according to our centre's standard hourly rate.

607 *Surgical Procedure*

608 Bilateral DBS (3389 Medtronic/Boston Vercise leads) implantation was performed
609 under general anaesthesia using a stereotactic MRI-guided and MRI-verified
610 approach without microelectrode recording (Leksell frame G, Elekta) as detailed in
611 previous publications (67,68). Two stereotactic, preimplantation scans were
612 acquired, as part of the surgical procedure, to guide lead implantation; a T2-weighted
613 axial scan (partial brain coverage around the STN) with voxel size of 1.0×1.0 mm2
614 (slice thickness=2 mm) and a T1-weighted 3D-MPRAGE scan with a (1.5 mm)3
615 voxel size on a 1.5T Siemens Espree interventional MRI scanner. Three dimensional
616 distortion correction was carried out using the scanner's built-in module. Target for
617 the deepest contact was selected at the level of maximal rubral diameter (~5 mm
618 below the AC-PC line). To maximise DBS trace within the STN, the target was often
619 chosen 1.5 - 2 mm posterolateral to that described by Bejjani (69). Stereotactic
620 imaging was repeated following lead implantation to confirm placement.

621 *Task*

622 To investigate the neural basis of evidence accumulation over time, we used the
623 expanded judgement task (Figure 1, similar to a task previously used by Leimbach et
624 al, 2018). Participants were shown a series of images of a mouse facing either left or
625 right. Cues were presented for 200ms, with an inter-stimulus interval (ISI) of 600ms,
626 so there was 800ms interval from one onset to another, to which we refer as Stimulus
627 Onset Asynchrony (SOA). Participants were required to judge in which direction the
628 mouse will 'run', based on the probabilities extracted from a series of sequential cue
629 images, and then respond accordingly. The validity of the cues was 70%, such that
630 each cue (left or right mouse) represented the correct choice 70% of the time. The two
631 directions were equally likely across trials, thus chance level in the task was 50%. If
632 the participants responded based on one of the cues only, without accumulating
633 information over time, then their expected success rate would be 70%. Responses
634 were made by pressing a button with the thumb of the congruent hand after a self-
635 chosen number of cues, when the participant felt they had enough evidence to make
636 a decision. Prior to the recording, the participants underwent a short training session
637 where they were first asked to respond only after seeing a set number of stimuli
638 (between two and ten) and then told that for the main experiment they will decide

639 themselves how many stimuli to observe. This was to ensure that participants made a
640 response decision based on accumulating evidence from a sequence of images rather
641 than just the first stimulus. Participants performed up to 200 trials (Patients: 168±11;
642 Controls: 200 each, except one control who completed 150 trials). Two patients were
643 excluded from the analysis due to poor performance of the task (accuracy at chance
644 level).

645 *Recording and Analysis*

646 Participants performed the task while seated in a whole-head MEG system (CTF-VSM
647 275-channel scanner, Coquitlam, Canada). For patients, STN-LFP,
648 electrooculography (EOG) and electromyography (EMG) recordings were also
649 obtained using a battery-powered and optically isolated EEG amplifier (BrainAmp MR,
650 Brain Products GmbH, Gilching, Germany). STN-LFP signals were recorded
651 referenced to a common cephalic reference (right mastoid).

652 All preprocessing was performed in SPM12 (v. 7771, http://www.fil.ion.ucl.ac.uk/spm/,
653 (70)), and spectral analysis and statistical tests were performed in Fieldtrip
654 (http://www.ru.nl/neuroimaging/fieldtrip/,(71)) using the version included in SPM12.

655 STN-LFP recordings were converted offline to a bipolar montage between adjacent
656 contacts (three bipolar channels per hemisphere; 01, 12, and 23) to limit the effects of
657 volume conduction from distant sources (for more details see Litvak et al. (2010),
658 Oswal et al (2016)). Four of the patients had segmented DBS leads (Vercise^{TM} DBS
659 directional lead, Boston Scientific, Marlborough, USA). In these cases, we averaged
660 offline the signals from the 3 segments of each ring and treated them as a single ring
661 contact. Thus, for each participant we had a total of 3 STN EEG channels in each
662 hemisphere (except for 2 participants: one with right side electrodes only, thus 3
663 channels, and one with 1 contact on the right excluded due to extensive noise, thus 5
664 channels). The LFP data were downsampled to 300Hz and high-pass filtered at 1Hz
665 (Butterworth 5th order, zero phase filter).

666 The SOA was fixed making entrainment and anticipation possible. These were
667 deliberate design choices to make the task easier for this very difficult patient
668 population prone to attentional difficulties, and to be able to collect a large number of
669 trials for model-based analyses. Any jittering of the SOAs (which would have to go in
670 the direction of increasing their duration) would have led to far fewer trials being

collected. The total duration of the recording had to be kept short as the patients were unable to tolerate extended periods of testing. Furthermore, having very long SOA would make it more likely that the participants would resort to explicit counting, which was something we aimed to avoid.

A possibly problematic but unavoidable feature of our task was that the stimuli were presented at relatively short SOA not allowing for the power to return to baseline before the next stimulus was presented (see Supplemental Methods for details). To account for these design issues, we developed an unconventional way of performing time-frequency analysis on these data in the absence of a baseline. We first ran time frequency analysis on continuous LFP data (multitaper method (73) 400ms sliding window, in steps of 50ms) on *a priori* defined beta power (13-30 Hz average = 21.5Hz; note that when looking at individual participant beta power around the response period, we found a similar band as defined *a priori*: individual mean range: 16.6-28.4Hz; overall min: 11Hz, max: 31Hz). Separately we also estimated the power in the theta band (2-8Hz average = 5Hz, e.g. Herz et al., 2016). The resulting power time series were log-transformed and high-pass filtered at 0.5 Hz (Butterworth 5th order, zero phase filter) to remove fluctuations in power that were slower than our SOA. Afterwards, the power time series were epoched around the presentation of each cue stimulus (-500 to 800ms). We averaged power across contacts within each hemisphere, resulting in 1 left and 1 right STN channel, and we also calculated the mean STN signal by combining hemispheres. For completeness we report individual contact data in the Supplementary Material (Supplementary Figure 1). We used a permutation cluster-based non-parametric test to correct for multiple comparisons across time (the duration of the whole cue epoch (0-800ms) and report effects that survive correction only ($p<0.05$ family-wise error (FWE) corrected at the cluster level).

Similarly to LFP, MEG data were downsampled to 300Hz, and high-pass filtered at 1Hz (Butterworth 5th order, zero phase filter). For sensor-level analysis only, we used the temporal extension of Signal Space Separation method (tSSS), (74), to remove the artefacts generated by the presence of ferromagnetic wires (75) from the MEG data (see Supplemental Material). Using tSSS we also realigned all the head locations to the average location of the control group. For consistency, tSSS preprocessing was applied to both patient and control MEG data. The code we used was an extension to CTF data of the Matlab prototype code for the commercial MaxFilterTM tSSS

implementation. The extension was done by the original developer (Samu Taulu) in collaboration with our group and publicly released by MEGIN Oy (Helsinki, Finland). This code is included in SPM12 as 'tSSS toolbox' and its detailed validation on CTF phantom data and comparison to other methods for DBS artefact removal has recently been published by Kandemir et al. (76)

For the MEG sensor-level time-frequency analysis, we used all channels and a frequency range of 1-45Hz. All other analyses were identical to the LFP pipeline reported above. However, we corrected for multiple comparisons across all MEG channels, timepoints (0-800ms) and frequencies (1-45Hz), and only report effects that survived that correction ($p<0.05$ FWE corrected at the cluster level).

At the source level, the continuous MEG data were projected to source space with Linearly Constrained Maximum Variance (LCMV) beamformer (77) using a 10-fold reduced version of the SPM canonical cortical mesh (78) as the source space (resulting in 818 vertices and the same number of source channels). The source orientation was set in the direction of maximum power. See Litvak et al. (2012) for details on beamforming and Litvak et al. (2010) for details on issues regarding beamformer use for removing artefacts from simultaneous MEG and intracranial recordings. Next, time frequency analysis was performed on continuous source data the same way as for STN-LFP except the frequencies of interest were informed by the sensor-level analysis. This biased the statistical test for discovery of an effect (cf. double dipping, Kriegeskorte, Simmons, Bellgowan, & Baker, 2009) but our aim in this analysis was post-hoc interrogation of the effects established at the sensor level in terms of their location in the cortex rather than hypothesis testing (80). Time-resolved coherence was then computed between the identified cortical sources and STN contacts by going back to raw source time series. The data were epoched (-1000 to 1000ms to increase the window for analysis), and time-frequency analysis was performed as described above with coherence between the sources and the left and right STN also computed from the cross-spectrum. Non-parametric permutation testing between conditions was corrected for multiple comparisons across channels (source vertices), time (0-600ms, note the cue epoch is 0-800ms, however due to the limits of the temporal resolution of the 400ms sliding window, we limited our analysis to the window of uncontaminated data) and frequencies (1-30Hz), and we only report effects that survive correction ($p<0.05$ FWE corrected at the cluster level).

Reconstruction of electrode locations

We used the Lead-DBS toolbox (http://www.lead-dbs.org/, (81)) to reconstruct the contact locations. Post-operative T2 and T1 images were co-registered to pre-operative T1 scan using linear registration in SPM12 (82). Pre- (and post-) operative acquisitions were spatially normalized into MNI_ICBM_2009b_NLIN_ASYM space based on preoperative T1 using the Unified Segmentation Approach as implemented in SPM12 (83). DBS electrode localizations were corrected for brain shift in postoperative acquisitions by applying a refined affine transform calculated between pre- and post-operative acquisitions that were restricted to a subcortical area of interest as implemented in the brain shift correction module of Lead-DBS software. The electrodes were then manually localized based on post-operative acquisitions using a tool in Lead-DBS specifically designed for this task. The resulting locations were verified by an expert neurosurgeon.

Data availability

The full MEG dataset for controls is available in BIDS format on https://openneuro.org/datasets/ds002908 and LFP and source data for patients is available on https://data.mrc.ox.ac.uk/data-set/human-lfp-recordings-stn-during-sequential-conflict-task. Code and analysis pipeline at https://github.com/zits69/MOUSE_LFPMEG.

Acknowledgements & Funding

This work has been supported by MRC grants MC_UU_12024/5, MC_UU_00003/1 and BBSRC grant BB/S006338/1. The Wellcome Centre for Human Neuroimaging is supported by core funding from the Wellcome (203147/Z/16/Z). UK MEG community is supported by UK MEG Partnership award from the Medical Research Council (MR/K005464/1). We thank Dr. Ashwini Oswal, Dr. Simon Little, Dr. David Pedrosa, Dr. Damian Herz and Dr. Viswas Dayal for clinical support of patient recordings. We are also grateful to Dr. Tim West, Dr. Hayriye Cagnan and Dr. Simon Farmer for commenting on the manuscript.

Competing interests None.

768 **REFERENCES**

769 1. Usher M, McClelland JL. The time course of perceptual choice: The leaky,
770 competing accumulator model. Psychol Rev. 2001;108(3):550–92.

771 2. Busemeyer JR, Townsend JT. Decision field theory: A dynamic-cognitive
772 approach to decision making in an uncertain environment. Psychol Rev.
773 1993;100(3):432–59.

774 3. Ratcliff R. A theory of memory retrieval. Psychol Rev. 1978;85(2):59–108.

775 4. Bogacz R, Wagenmakers E-J, Forstmann BU, Nieuwenhuis S. The neural
776 basis of the speed-accuracy tradeoff. Trends Neurosci [Internet].
777 2010;33(1):10–6. Available from:
778 http://www.ncbi.nlm.nih.gov/pubmed/19819033

779 5. Frank MJ. Hold your horses: A dynamic computational role for the subthalamic
780 nucleus in decision making. Neural Networks. 2006;19(8):1120–36.

781 6. Green N, Bogacz R, Huebl J, Beyer AK, Kühn AA, Heekeren HR. Reduction of
782 influence of task difficulty on perceptual decision making by stn deep brain
783 stimulation. Curr Biol. 2013;23(17):1681–4.

784 7. Coulthard EJ, Bogacz R, Javed S, Mooney LK, Murphy G, Keeley S, et al.
785 Distinct roles of dopamine and subthalamic nucleus in learning and
786 probabilistic decision making. Brain. 2012 Dec;135(Pt 12):3721–34.

787 8. Frank MJ, Samanta J, Moustafa AA, Sherman SJ. Hold your horses:
788 Impulsivity, deep brain stimulation, and medication in Parkinsonism. Science
789 (80-) [Internet]. 2007;318(5854):1309–12. Available from:
790 http://www.ncbi.nlm.nih.gov/pubmed/17962524

791 9. Cavanagh JF, Wiecki T V., Cohen MX, Figueroa CM, Samanta J, Sherman SJ,
792 et al. Subthalamic nucleus stimulation reverses mediofrontal influence over
793 decision threshold. Nat Neurosci [Internet]. 2011;14(11):1462–7. Available
794 from: http://dx.doi.org/10.1038/nn.2925

795 10. Herz DM, Zavala B, Bogacz R, Brown P. Neural Correlates of Decision
796 Thresholds in the Human Subthalamic Nucleus. Curr Biol [Internet].
797 2016;26(7):916–20. Available from: http://dx.doi.org/10.1016/j.cub.2016.01.051

11. Bonnevie T, Zaghloul KA. The Subthalamic Nucleus: Unravelling New Roles and Mechanisms in the Control of Action. Neuroscientist. 2019;25(1):48–64.

12. Zavala B, Damera S, Dong JW, Lungu C, Brown P, Zaghloul KA. Human subthalamic nucleus theta and beta oscillations entrain neuronal firing during sensorimotor conflict. Cereb Cortex. 2015;27(1):496–508.

13. Benis D, David O, Lachaux JP, Seigneuret E, Krack P, Fraix V, et al. Subthalamic nucleus activity dissociates proactive and reactive inhibition in patients with Parkinson's disease. Neuroimage [Internet]. 2014;91:273–81. Available from: http://dx.doi.org/10.1016/j.neuroimage.2013.10.070

14. Alegre M, Lopez-Azcarate J, Obeso I, Wilkinson L, Rodriguez-Oroz MC, Valencia M, et al. The subthalamic nucleus is involved in successful inhibition in the stop-signal task: A local field potential study in Parkinson's disease. Exp Neurol [Internet]. 2013;239(1):1–12. Available from: http://dx.doi.org/10.1016/j.expneurol.2012.08.027

15. Ray NJ, Brittain J-S, Holland P, Joundi RA, Stein JF, Aziz TZ, et al. The role of the subthalamic nucleus in response inhibition: Evidence from local field potential recordings in the human subthalamic nucleus. Neuroimage [Internet]. 2012;60(1):271–8. Available from: http://dx.doi.org/10.1016/j.neuroimage.2011.12.035

16. Brittain J-S, Watkins KE, Joundi RA, Ray NJ, Holland P, Green AL, et al. A role for the subthalamic nucleus in response inhibition during conflict. J Neurosci. 2012;32(39):13396–401.

17. Jahanshahi M. Effects of deep brain stimulation of the subthalamic nucleus on inhibitory and executive control over prepotent responses in Parkinson's disease. Front Syst Neurosci. 2013;7(December):118.

18. Herz DM, Little S, Pedrosa DJ, Tinkhauser G, Cheeran B, Foltynie T, et al. Mechanisms Underlying Decision-Making as Revealed by Deep-Brain Stimulation in Patients with Parkinson's Disease. Curr Biol [Internet]. 2018;28(8):1169-1178.e6. Available from: https://doi.org/10.1016/j.cub.2018.02.057

19. Antonelli F, Ko JH, Miyasaki J, Lang AE, Houle S, Valzania F, et al. Dopamine-agonists and impulsivity in Parkinson's disease: Impulsive choices vs. impulsive actions. Hum Brain Mapp. 2014;35(6):2499–506.

20. Voon V, Mehta AR, Hallett M. Impulse control disorders in Parkinson's disease: recent advances. Curr Opin Neurol [Internet]. 2011 Aug;24(4):324–30. Available from: https://pubmed.ncbi.nlm.nih.gov/21725242

21. Aarsland D, Creese B, Politis M, Chaudhuri KR, Ffytche DH, Weintraub D, et al. Cognitive decline in Parkinson disease. Nat Rev Neurol. 2017;13(4):217–31.

22. Mosley PE, Paliwal S, Robinson K, Coyne T, Silburn P, Tittgemeyer M, et al. The structural connectivity of subthalamic deep brain stimulation correlates with impulsivity in Parkinson's disease. Brain. 2020;143(7):2235–54.

23. Litvak V, Jha A, Eusebio A, Oostenveld R, Foltynie T, Limousin P, et al. Resting oscillatory cortico-subthalamic connectivity in patients with Parkinson's disease. Brain. 2011;134(2):359–74.

24. Magill PJ, Sharott A, Bolam JP, Brown P. Brain state-dependency of coherent oscillatory activity in the cerebral cortex and basal ganglia of the rat. J Neurophysiol. 2004;92(4):2122–36.

25. West TO, Farmer SF, Magill PJ, Sharott A, Litvak V, Cagnan H. State Dependency of Beta Oscillations in the Cortico-Basal-Ganglia Circuit and their Neuromodulation under Phase Locked Inputs. 2020;(March):1–42.

26. West TO, Berthouze L, Halliday DM, Litvak V, Sharott A, Magill PJ, et al. Propagation of beta/gamma rhythms in the cortico-basal ganglia circuits of the parkinsonian rat. J Neurophysiol. 2018;119(5):1608–28.

27. Zavala B, Tan H, Ashkan K, Foltynie T, Limousin P, Zrinzo L, et al. Human subthalamic nucleus-medial frontal cortex theta phase coherence is involved in conflict and error related cortical monitoring. Neuroimage [Internet]. 2016;137:178–87. Available from: http://dx.doi.org/10.1016/j.neuroimage.2016.05.031

28. Zavala B, Tan H, Little S, Ashkan K, Hariz M, Foltynie T, et al. Midline frontal

858 cortex low-frequency activity drives subthalamic nucleus oscillations during
859 conflict. J Neurosci. 2014 May;34(21):7322–33.

860 29. Leimbach F, Georgiev D, Litvak V, Antoniades C, Limousin P, Jahanshahi M,
861 et al. Deep brain stimulation of the subthalamic nucleus does not affect the
862 decrease of decision threshold during the choice process when there is no
863 conflict, time pressure, or reward. J Cogn Neurosci [Internet]. 2018 Feb
864 28;30(6):876–84. Available from: https://doi.org/10.1162/jocn_a_01252

865 30. Horn A, Neumann W-J, Degen K, Schneider G-H, Kühn AA. Toward an
866 electrophysiological "sweet spot" for deep brain stimulation in the subthalamic
867 nucleus. Hum Brain Mapp. 2017 Jul;38(7):3377–90.

868 31. van Wijk BCM, Pogosyan A, Hariz MI, Akram H, Foltynie T, Limousin P, et al.
869 Localization of beta and high-frequency oscillations within the subthalamic
870 nucleus region. NeuroImage Clin [Internet]. 2017;16(April):175–83. Available
871 from: https://doi.org/10.1016/j.nicl.2017.07.018

872 32. Milosevic L, Scherer M, Cebi I, Guggenberger R, Machetanz K, Naros G, et al.
873 Online Mapping with the Deep Brain Stimulation Lead: A Novel Targeting Tool
874 in Parkinson's Disease. Mov Disord [Internet]. 2020 May 18;n/a(n/a). Available
875 from: https://doi.org/10.1002/mds.28093

876 33. Ewert S, Plettig P, Li N, Chakravarty MM, Collins DL, Herrington TM, et al.
877 Toward defining deep brain stimulation targets in MNI space: A subcortical
878 atlas based on multimodal MRI, histology and structural connectivity.
879 Neuroimage. 2018 Apr;170:271–82.

880 34. Bogacz R, Gurney K. The basal ganglia and cortex implement optimal
881 decision. Neural Comput. 2007 Feb;19(2):442–77.

882 35. Gould IC, Nobre AC, Wyart V, Rushworth MFS. Effects of decision variables
883 and intraparietal stimulation on sensorimotor oscillatory activity in the human
884 brain. J Neurosci. 2012;32(40):13805–18.

885 36. Zavala B, Jang AI, Zaghloul KA. Human subthalamic nucleus activity during
886 non-motor decision making. Elife. 2017;6:1–23.

887 37. Bogacz R, Martin Moraud E, Abdi A, Magill PJ, Baufreton J. Properties of

Neurons in External Globus Pallidus Can Support Optimal Action Selection. PLoS Comput Biol. 2016;12(7):1–28.

38. Wessel JR, Jenkinson N, Brittain J-S, Voets SHEM, Aziz TZ, Aron AR. Surprise disrupts cognition via a fronto-basal ganglia suppressive mechanism. Nat Commun. 2016;7.

39. Keuken MC, Van Maanen L, Bogacz R, Schäfer A, Neumann J, Turner R, et al. The subthalamic nucleus during decision-making with multiple alternatives. Hum Brain Mapp. 2015;36(10):4041–52.

40. Zavala B, Jang A, Trotta M, Lungu CI, Brown P, Zaghloul KA. Cognitive control involves theta power within trials and beta power across trials in the prefrontal-subthalamic network. Brain. 2018;141(12):3361–76.

41. Ruiz MH, Rusconi M, Brücke C, Haynes JD, Schönecker T, Kühn AA. Encoding of sequence boundaries in the subthalamic nucleus of patients with Parkinson's disease. Brain. 2014;137(10):2715–30.

42. Chen W, de Hemptinne C, Miller AM, Leibbrand M, Little SJ, Lim DA, et al. Prefrontal-Subthalamic Hyperdirect Pathway Modulates Movement Inhibition in Humans. Neuron [Internet]. 2020;106(4):579-588.e3. Available from: https://doi.org/10.1016/j.neuron.2020.02.012

43. Fife KH, Gutierrez-Reed NA, Zell V, Bailly J, Lewis CM, Aron AR, et al. Causal role for the subthalamic nucleus in interrupting behavior. Elife. 2017;6:1–13.

44. Pavlides A, Hogan SJ, Bogacz R. Computational Models Describing Possible Mechanisms for Generation of Excessive Beta Oscillations in Parkinson's Disease. PLoS Comput Biol. 2015;11(12):1–29.

45. Leventhal DK, Gage GJ, Schmidt R, Pettibone JR, Case AC, Berke JD. Basal ganglia beta oscillations accompany cue utilization. Neuron [Internet]. 2012;73(3):523–36. Available from: http://dx.doi.org/10.1016/j.neuron.2011.11.032

46. Muthukumaraswamy SD, Singh KD. A cautionary note on the interpretation of phase-locking estimates with concurrent changes in power. Clin Neurophysiol [Internet]. 2011;122(11):2324–5. Available from:

http://www.sciencedirect.com/science/article/pii/S1388245711002598

47. Wessel JR, Waller DA, Greenlee JD. Non-selective inhibition of inappropriate motor-tendencies during response-conflict by a fronto-subthalamic mechanism. Elife. 2019;8:1–26.

48. Aron AR. From reactive to proactive and selective control: Developing a richer model for stopping inappropriate responses. Biol Psychiatry [Internet]. 2011;69(12):e55–68. Available from: http://dx.doi.org/10.1016/j.biopsych.2010.07.024

49. Chambers CD, Bellgrove MA, Gould IC, English T, Garavan H, McNaught E, et al. Dissociable mechanisms of cognitive control in prefrontal and premotor cortex. J Neurophysiol. 2007;98(6):3638–47.

50. Simmonds DJ, Pekar JJ, Mostofsky SH. Meta-analysis of Go/No-go tasks demonstrating that fMRI activation associated with response inhibition is task-dependent. Neuropsychologia. 2008;46(1):224–32.

51. DeLong MR. Primate models of movement disorders of basal ganglia origin. Trends Neurosci. 1990;13(7):281–5.

52. Albin RL, Young AB, Penney JB. The functional anatomy of basal ganglia disorders. Trends Neurosci [Internet]. 1989;12(10):366–75. Available from: http://www.sciencedirect.com/science/article/pii/016622368990074X

53. Nambu A, Tokuno H, Takada M. Functional significance of the cortico-subthalamo-pallidal “hyperdirect” pathway. Neurosci Res. 2002;43(2):111–7.

54. Oswal A, Beudel M, Zrinzo L, Limousin P, Hariz M, Foltynie T, et al. Deep brain stimulation modulates synchrony within spatially and spectrally distinct resting state networks in Parkinson’s disease. Brain. 2016;139(5):1482–96.

55. Aron AR, Robbins TW, Poldrack RA. Right inferior frontal cortex: Addressing the rebuttals. Front Hum Neurosci. 2014;8(November):8–11.

56. Hampshire A. Putting the brakes on inhibitory models of frontal lobe function. Neuroimage [Internet]. 2015;113:340–55. Available from: http://dx.doi.org/10.1016/j.neuroimage.2015.03.053

57. Erika-Florence M, Leech R, Hampshire A. A functional network perspective on response inhibition and attentional control. Nat Commun [Internet]. 2014;5(May):1–12. Available from: http://dx.doi.org/10.1038/ncomms5073

58. Cavanagh JF, Frank MJ. Frontal theta as a mechanism for cognitive control. Trends Cogn Sci [Internet]. 2014;18(8):414–21. Available from: http://dx.doi.org/10.1016/j.tics.2014.04.012

59. Bastin J, Polosan M, Benis D, Goetz L, Bhattacharjee M, Piallat B, et al. Inhibitory control and error monitoring by human subthalamic neurons. Transl Psychiatry. 2014;4(9):2–9.

60. Zuure MB, Hinkley LBN, Tiesinga PHE, Nagarajan SS, Cohen MX. Multiple midfrontal thetas revealed by source separation of simultaneous MEG and EEG. bioRxiv [Internet]. 2020 Jan 1;2020.03.11.987040. Available from: http://biorxiv.org/content/early/2020/03/11/2020.03.11.987040.abstract

61. Bogacz R, Larsen T. Integration of reinforcement learning and optimal decision-making theories of the basal ganglia. Neural Comput. 2011;23(4):817–51.

62. Brunton BW, Botvinick MM, Brody CD. Rats and Humans Can Optimally Accumulate Evidence for Decision-Making. Science (80-). 2013;340(April):95–9.

63. Hershey T, Campbell MC, Videen TO, Lugar HM, Weaver PM, Hartlein J, et al. Mapping Go-No-Go performance within the subthalamic nucleus region. Brain. 2010;133(12):3625–34.

64. De Lange FP, Jensen O, Dehaene S. Accumulation of evidence during sequential decision making: The importance of top-down factors. J Neurosci. 2010;30(2):731–8.

65. Gould IC, Rushworth MF, Nobre AC. Indexing the graded allocation of visuospatial attention using anticipatory alpha oscillations. J Neurophysiol [Internet]. 2011 Mar [cited 2013 Apr 6];105(3):1318–26. Available from: http://www.pubmedcentral.nih.gov/articlerender.fcgi?artid=3074422&tool=pmcentrez&rendertype=abstract

66. Foltynie T, Zrinzo L, Martinez-Torres I, Tripoliti E, Petersen E, Holl E, et al. MRI-guided STN DBS in Parkinson's disease without microelectrode recording: Efficacy and safety. J Neurol Neurosurg Psychiatry. 2011;82(4):358–63.

67. Holl EM, Petersen EA, Foltynie T, Martinez-Torres I, Limousin P, Hariz MI, et al. Improving Targeting in Image-Guided Frame-Based Deep Brain Stimulation. Oper Neurosurg [Internet]. 2010 Dec 1;67(suppl_2):ons437–47. Available from: https://doi.org/10.1227/NEU.0b013e3181f7422a

68. Foltynie T, Zrinzo L, Martinez-Torres I, Tripoliti E, Petersen E, Holl E, et al. MRI-guided STN DBS in Parkinson's disease without microelectrode recording: efficacy and safety. J Neurol Neurosurg Psychiatry. 2011 Apr;82(4):358–63.

69. Bejjani B-P, Dormont D, Pidoux B, Yelnik J, Damier P, Arnulf I, et al. Bilateral subthalamic stimulation for Parkinson's disease by using three-dimensional stereotactic magnetic resonance imaging and electrophysiological guidance. J Neurosurg [Internet]. 2000;92(4):615–25. Available from: https://thejns.org/view/journals/j-neurosurg/92/4/article-p615.xml

70. Litvak V, Mattout J, Kiebel S, Phillips C, Henson R, Kilner J, et al. EEG and MEG data analysis in SPM8. Baillet S, editor. Comput Intell Neurosci [Internet]. 2011 Jan [cited 2011 Jul 7];2011:852961. Available from: https://doi.org/10.1155/2011/852961

71. Oostenveld R, Fries P, Maris E, Schoffelen J-MM. FieldTrip: Open source software for advanced analysis of MEG, EEG, and invasive electrophysiological data. Comput Intell Neurosci [Internet]. 2011 Jan [cited 2012 Mar 9];2011:156869. Available from: http://www.pubmedcentral.nih.gov/articlerender.fcgi?artid=3021840&tool=pmcentrez&rendertype=abstract

72. Oswal A, Jha A, Neal S, Reid A, Bradbury D, Aston P, et al. Analysis of simultaneous MEG and intracranial LFP recordings during Deep Brain Stimulation: A protocol and experimental validation. J Neurosci Methods [Internet]. 2016;261:29–46. Available from:

http://dx.doi.org/10.1016/j.jneumeth.2015.11.029

73. Thomson DJ. Spectrum estimation and harmonic analysis. Proc IEEE. 1982;70(9):1055–96.

74. Taulu S, Hari R. Removal of magnetoencephalographic artifacts with temporal signal-space separation: demonstration with single-trial auditory-evoked responses. Hum Brain Mapp. 2009;30(5):1524–34.

75. Litvak V, Eusebio A, Jha A, Oostenveld R, Barnes GR, Penny WD, et al. Optimized beamforming for simultaneous MEG and intracranial local field potential recordings in deep brain stimulation patients. Neuroimage [Internet]. 2010;50(4):1578–88. Available from: http://dx.doi.org/10.1016/j.neuroimage.2009.12.115

76. Kandemir AL, Litvak V, Florin E. The comparative performance of DBS artefact rejection methods for MEG recordings. Neuroimage [Internet]. 2020 Oct;219:117057. Available from: https://doi.org/10.1016/j.neuroimage.2020.117057

77. Veen BD Van, Drongelen W Van, Yuchtman M, Suzuki A. Localization of brain electrical activity via linearly constrained minimum variance spatial filtering. IEEE Trans Biomed Eng. 1997;44(9):867–80.

78. Mattout J, Henson RN, Friston KJ. Canonical Source Reconstruction for MEG. Sanei S, editor. Comput Intell Neurosci [Internet]. 2007;2007:67613. Available from: https://doi.org/10.1155/2007/67613

79. Kriegeskorte N, Simmons WK, Bellgowan PS, Baker CI. Circular analysis in systems neuroscience: The dangers of double dipping. Nat Neurosci. 2009;12(5):535–40.

80. Gross J, Baillet S, Barnes GR, Henson RN, Hillebrand A, Jensen O, et al. Good practice for conducting and reporting MEG research. Neuroimage [Internet]. 2012 Oct 6;65C:349–63. Available from: http://www.ncbi.nlm.nih.gov/pubmed/23046981

81. Horn A, Kühn AA. Lead-DBS: a toolbox for deep brain stimulation electrode localizations and visualizations. Neuroimage. 2015;107:127–35.

82. Friston KJ (Karl J., Ashburner J, Kiebel S, Nichols T, Penny WD. Statistical parametric mapping : the analysis of funtional brain images. Elsevier/Academic Press; 2007. 647 p.

83. Ashburner J, Friston KJ. Unified segmentation. Neuroimage [Internet]. 2005 Jul 1 [cited 2011 Jun 11];26(3):839–51. Available from: http://www.ncbi.nlm.nih.gov/pubmed/15955494

Supplemental Material

Estimating accumulated evidence using computational models

To provide more precise description of STN activity and formal hypotheses on its function, computational models have been developed (Bogacz & Gurney, 2007; Frank, 2006). In particular, one model suggests that the basal ganglia compute the reward probabilities for selecting different actions according to Bayesian decision theory (Bogacz & Gurney, 2007; Bogacz & Larsen, 2011). These probabilities are updated after each stimulus and the updated information is fed back to the cortex via the thalamus. An action is initiated when the expected reward under a particular action exceeds a certain threshold. The model attributes a very specific function to the STN: ensuring that if the probability of one action goes up, the probabilities of the others go down at the same time by normalising all probabilities so that they add up to one. The model makes precise predictions on how the STN activity should depend on the sequence of sensory evidence presented so far, but it has not been possible to test these predictions using the data from existing studies.

In order to analyse if STN activity reflects the amount of available evidence for each response based on the stimuli presented so far or the Bayesian normalization term (Bogacz & Gurney, 2007), we employed computational models that can estimate these quantities at each point in time. We compared how well different models of evidence accumulation could capture behaviour of different patients, and then generated regressors for each patient based on the best model for that patient.

A basic model in Equation 1 continuously updates the evidence (decision variable, *DV*) for a choice at time *t* based on the existing *DV* from the previous stimuli and the new incoming stimulus S_t, where $S_t = -1$ for the left stimulus, and $S_t = 1$ for the right stimulus. At the start of each trial, the decision variable was initialized to $DV_0 = 0$, and as the decision variable took values further from zero, the probability of making a response increased (see below).

$$DV_t = DV_{t-1} + S_t \quad (1)$$

$$DV_t = (1 - \lambda)DV_{t-1} + S_t \quad (2)$$

$$DV_t = DV_{t-1} + \omega_t S_t \quad (3)$$

$$DV_t = (1 - \lambda)DV_{t-1} + \omega_t S_t \quad (4)$$

We also considered three extended models which included a forgetting term (λ), a bonus term (ω), or both (Equations 2-4). The forgetting term was used to model the decay of memory over the course of the trial and the bonus term is a weighting of ‘same’ pairs, i.e. the stimuli which

match the directly preceding one (e.g.: in a ‘left-left-right’ sequence the second left stimulus would be weighted extra as it is the same as the first one).

To estimate the parameters, we assumed that the ratio of making a right choice to making a left choice is related to decision variable according to:

$$\log \frac{P(right)}{P(left)} = \beta_0 + \beta_t DV_t$$

For each participant, we looked for parameters that maximized the likelihood of participant’s behaviour after all stimuli shown to that participant.

We found the winning model (based on Bayesian information criterion) to be variable across participants (number of participants in patients/control group indicated): M1 = 1/0; M2 = 0/0; M3 = 4/1; M4 = 8/8, although the model that included both forgetting and bonus terms was the most common. The value of $|DV_t|$ from the best model for a given patient was used as a regressor in Figure 5A.

Strategy Use

In order to analyse the strategy used by the participants, we investigated which factors influence commitment to a choice on a given trial. We considered two factors: The first of them is the evidence integrated for the chosen option according to Equation 1. The second factor we considered was whether the stimulus was the same as the previously presented one, i.e. $SA_t = 1$ if $S_t = S_{t-1}$ and $SA_t = 0$ otherwise. For all stimuli excluding the first stimulus on each trial (for which it is not possible to define SA_t) we performed a logistic regression predicting if the choice has been made after this stimulus, i.e. we tried to predict a variable $D_t = 1$ if choice made after stimulus t and $D_t = 0$ otherwise. For each participant we looked at the significance of the two factors.

There was no participant (among patients and controls) who had a significant second factor (‘same’ stimulus), but not significant the first factor (evidence). Hence there was no participant who exclusively relied of making a choice after seeing the ‘same’ stimulus, without considering evidence integrated so far.

	CONTROLS (n)	PATIENTS(n)
Integration	6	6
Combination of integration and pair responses	7	5
Responding to ‘same’	0	0
Neither category	0	2

Estimating Bayesian normalization term

In order to create regressors for neural activity recorded from the STN, we used the original proposal that the STN computes the normalization term of the Bayesian equation during the evidence integration process (Bogacz & Gurney, 2007). We defined 2 cortical integrators Y_L and Y_R, which integrate evidence for the left and right stimulus respectively, as described above. Additionally, we subtracted the STN normalization term from the cortical integrators after each stimulus input in a sequence (Bogacz et al., 2016). So, for example, for participants best described by Model 1, the integrators were updated as follows

$$Y_{L,t} = Y_{L,t-1} + L_t - STN_{t-1} \quad (5)$$

$$Y_{R,t} = Y_{R,t-1} + R_t - STN_{t-1} \quad (6)$$

$$STN_t = \log\left(\exp Y_{L,t} + \exp Y_{R,t}\right) \quad (7)$$

In the above equations, $L_t = 1$, $R_t = 0$ if cue t is left, and $L_t = 0$, $R_t = 1$, otherwise. However, for models 2-4 we added decay to the cortical integrators and bonus terms to Equations 5-6 analogously to Equation 2-4. At the start of each trial, the integrators were initialized to $Y_{L,0} = Y_{R,0} = \log 0.5$ (corresponding to equal prior probabilities of the two responses). The value computed from Equation 7 was used as Bayesian normalization regressor in Figure 5.

REFERENCES

Bogacz, R., & Gurney, K. (2007). The basal ganglia and cortex implement optimal decision. *Neural Computation*, *19*(2), 442–477.

Bogacz, R., & Larsen, T. (2011). Integration of reinforcement learning and optimal decision-making theories of the basal ganglia. *Neural Computation*, *23*(4), 817–851.

Bogacz, R., Martin Moraud, E., Abdi, A., Magill, P. J., & Baufreton, J. (2016). Properties of Neurons in External Globus Pallidus Can Support Optimal Action Selection. *PLoS Computational Biology*, *12*(7), 1–28.

Ewert, S., Plettig, P., Li, N., Chakravarty, M. M., Collins, D. L., Herrington, T. M., … Horn, A. (2018). Toward defining deep brain stimulation targets in MNI space: A subcortical atlas based on multimodal MRI, histology and structural connectivity. *NeuroImage*, *170*, 271–282.

Frank, M. J. (2006). Hold your horses: A dynamic computational role for the subthalamic nucleus in decision making. *Neural Networks*, *19*(8), 1120–1136.

Table 1: Behavioural Data and Follow-up Statistical Tests. Independent sample t-test revealed significant differences between groups for accuracy and reaction time (ACC: t = -2.99, df = 15.19, p-value = 0.009; RT: t = 2.16, df = 23.37, p-value = 0.041), but not number of stimuli sampled (t = 0.42, df = 23.62, p-value = 0.68). Both groups were similar in their tendency to respond after seeing a 'same' pair (Ratio of responses after 'same': t = -2.01, df = 22.19, p-value = 0.057). The analytical probability of a 'same' pair at the end of the sequence would be 58% if participants chose the moment of response randomly. Both patients and controls responded significantly more often after a 'same' pair (both p<0.001).

PATIENTS	# stimuli seen	ACC	RT(ms)	RT 'different'	RT 'same'	ACC 'different'	ACC 'same'	Ratio of responses after 'same' at end
Mean	6.59	0.80	566.07	533.30	608.17	0.65	0.84	0.73
SD	1.88	0.10	57.39	89.17	62.78	0.14	0.10	0.11
SEM	0.52	0.03	15.92	24.73	17.41	0.04	0.03	0.03
Median	6.29	0.84	578.03	572.54	611.90	0.63	0.88	0.78
Min	3.88	0.56	475.62	343.91	508.12	0.47	0.56	0.54
Max	10.12	0.89	650.86	645.10	704.00	0.89	0.94	0.88

CONTROLS	# stimuli seen	ACC	RT(ms)	RT 'different'	RT 'same'	ACC 'different'	ACC 'same'	Ratio of responses after 'same' at end
Mean	6.29	0.89	512.85	517.22	522.90	0.77	0.91	0.81
SD	1.65	0.04	67.78	89.75	69.76	0.14	0.03	0.09
SEM	0.46	0.01	18.80	24.89	19.35	0.04	0.01	0.02
Median	5.84	0.90	517.70	528.60	519.55	0.80	0.92	0.79
Min	4.13	0.83	416.90	379.88	416.34	0.42	0.86	0.67
Max	9.11	0.95	636.08	672.74	638.49	0.93	0.96	0.96

Table 2: Correlations between beta power (different – same) and coherence (different – same) and behavioural measures

Correlations	RT	# of samples (cues)	ACC
Cue ‘i’ (100-450ms)	r=0.43,p=0.15	r=0.3,p=0.32	r=-0.11,p=0.7
Cue ‘i+1’ (750-1100ms)	r=-0.49,p=0.09	r=-0.4,p=0.17	r=0.49,p=0.12
Cue ‘i+1’ (1300-1600ms)	r=0.16,p=0.6	r=0.17,p=0.58	r=-0.21,p=0.48
Coherence (0-240ms)	r=-0.29,p=0.33	r=-0.26,p=0.39	r=-0.41,p=0.16

Bonferroni correction: 0.05/12=0.0042;

We correlated across participants the changes in beta power at each cue (cue ‘i’, ‘i+1’, ‘i+2’) with behavioural measures (accuracy, reaction time, the number of stimuli sampled). We found a significant negative relationship (r=-.5, p=0.048) only between the reaction time and the difference in beta power between ‘different’ and ‘same’ at cue ‘i+1’ (averaged over the significant time window, i.e. 750-1100 ms after onset of cue i). However, this did not survive Bonferroni correction. When correlating trial-wise beta power with reaction time or the number of stimuli sampled at the single participant level, we did not find any significant effects.

Supplementary Figure 1: Effects from Figure 2, plotted for each STN contact separately, rather than averaged over all contacts. We did not find a correlation between contact location and the 'same'-'different' effect. Top: Beta power. Bottom: Theta power.

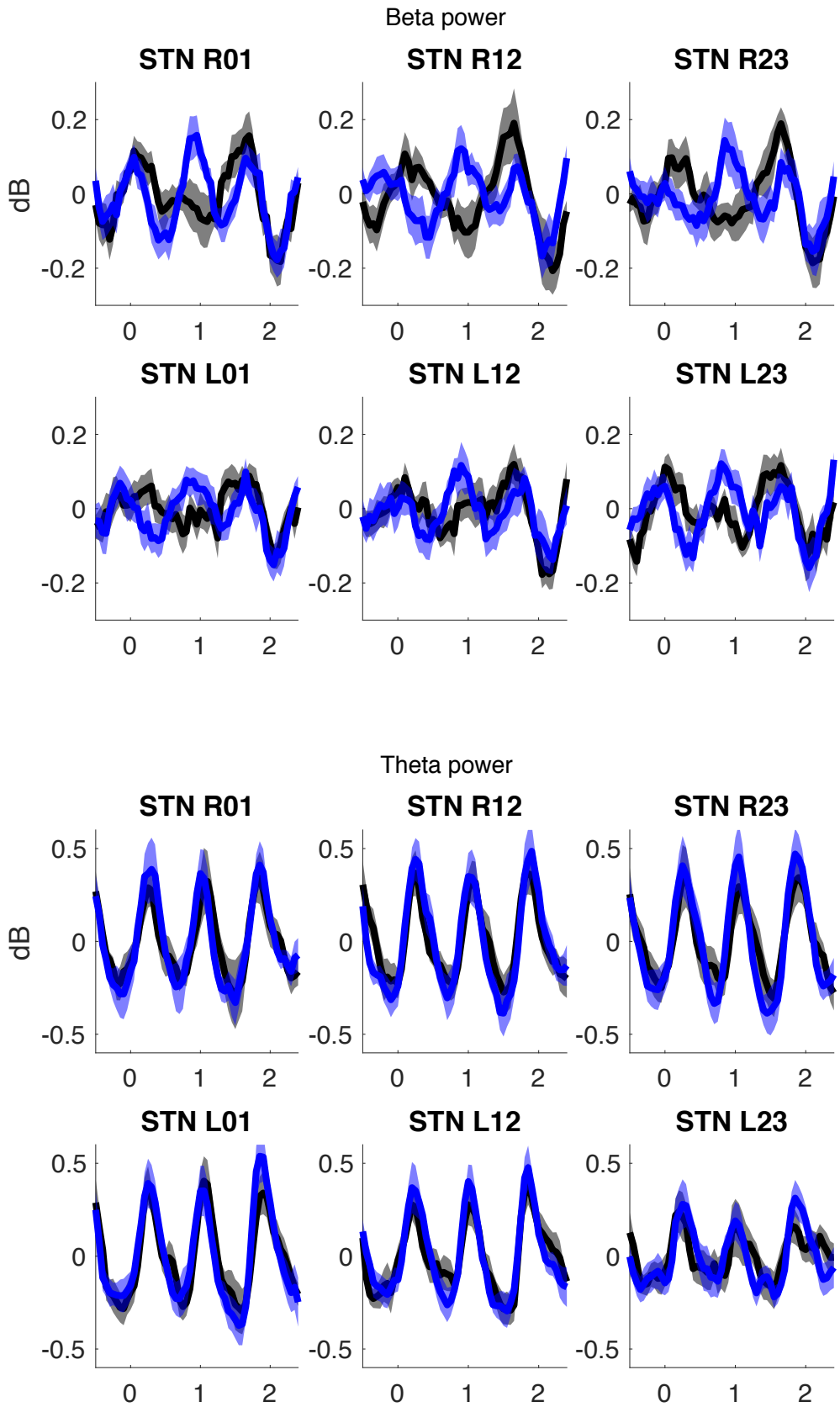

Supplementary Figure 2: Effects from Figure 2, plotted with cue i+1 in detail – for example: 'same'-'different' could be a cue sequence: 'L-L-R'. Plotted is the response to the last cue of the triplet, 'R', in this example. Top: Beta power. Bottom: Theta power.

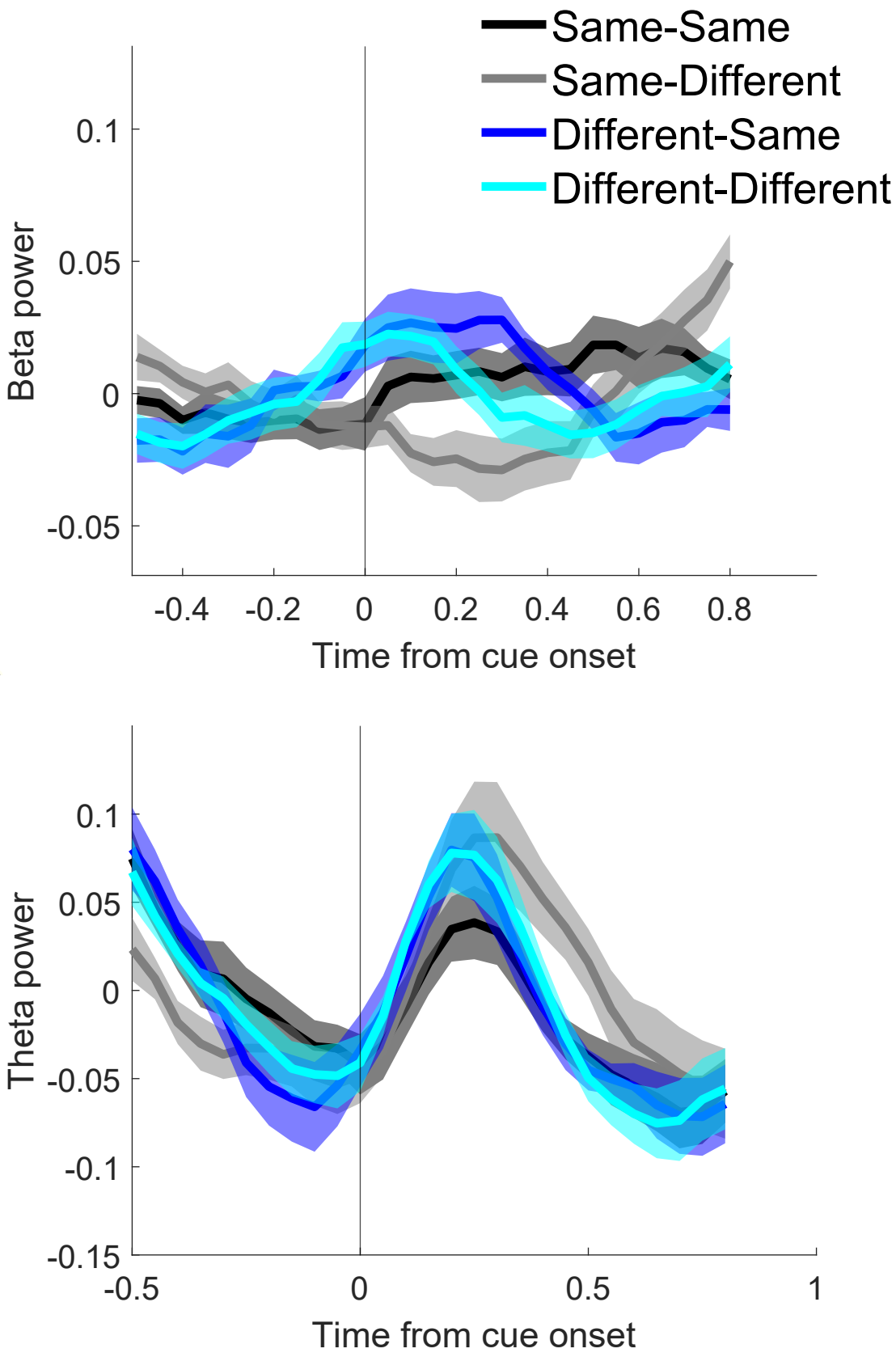

Supplementary Figure 3: Localization of DBS electrodes. Reconstructed electrode locations overlaid on structural atlas (Ewert et al., 2018) using Lead DBS toolbox (see Supplementary Methods). Top: STN: orange; Individual contacts shown for each participant; Globus Pallidus external: blue; Globus Pallidus internal: green; Red Nucleus: red. Bottom: Midpoint location of contact pair Right 1-2 superimposed on STN (coronal, axial, sagittal views -note radiological convention). The midpoint of contact pair Right 1-2 was within 0.5 mm (one contact length) from the nearest STN voxel for all patients and within 0.5 mm from the nearest voxel in the motor subdivision of the STN in 12 out of 13 patients. These results are based on DISTAL DBS functional zones atlas (Ewert et al., 2018)) and should be interpreted with caution as normalisation of subcortical anatomy to the template space does not always perfectly capture the variability of individual STN shapes.
Boston Vercise directional lead (left) and Medtronic 3386 (right) are plotted to scale for comparison, with scale bar showing 1mm.

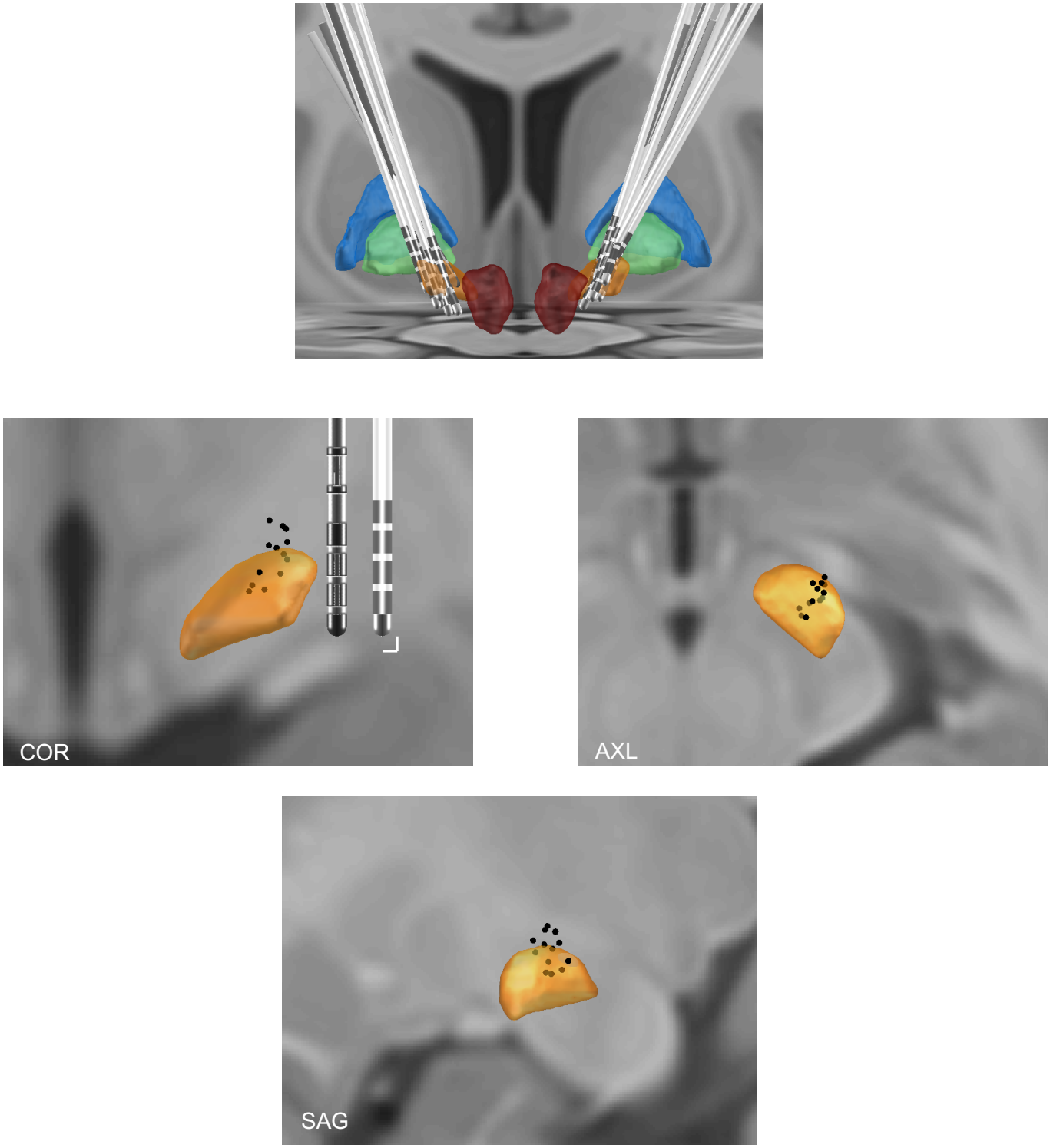
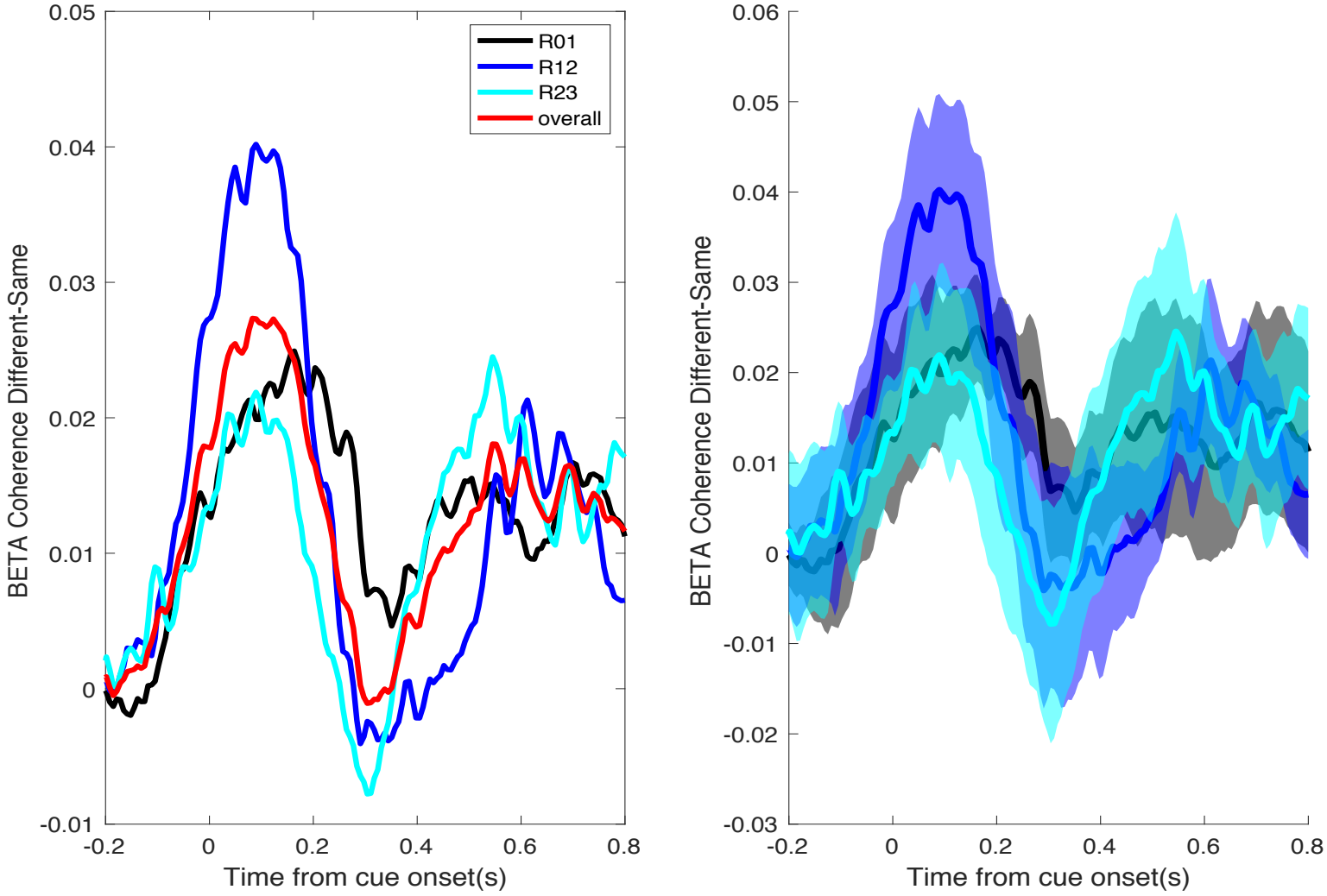
Supplementary Figure 4: Coherence plotted for each right STN contact. Left: The red line is the mean of all contacts, and is identical to the red line in Figure 6. **Right: same data as in left plot but with standard error of the mean plotted as well.**